POLITECNICO DI MILANO

Facoltà di Ingegneria Industriale

Corso di Laurea in
Ingegneria Meccanica

Robot Assisted Stapedotomy with
an Active Handheld Instrument

Relatore: Prof. Giovanni LEGNANI
Co-relatore: Prof. Elena DE MOMI
Co-relatore: Prof. Cameron N. RIVIERE

Tesi di Laurea di:
Tobia VEDRAMETTO Matr. 784086

Anno Accademico 2014 - 2015

This master thesis project was performed in collaboration with:

Carnegie Mellon University, The Robotics Institute

Surgical Mechatronics Lab

Supervisor:

Professor Cameron N. Riviere

And

Politecnico di Milano, Department of Electronics, Information and Bioengineering (DEIB)

NEARLab Medical Robotics

Supervisor:

Professor Elena De Momi

Acknowledgments

This thesis would not have been possible without the help of many people.

First, a big thank to professor Cameron Riviere and professor Elena De Momi, who gave me the possibility for this research, that transformed in my “American experience”, giving me life and technical knowledge. And with them all the other guys of the Mechatronics Surgical Lab: Nate Wood, Tent Wells, Craig Lehocky and in particular Sungwook Yang and Rob Maclachlan that helped me a lot, whatever and whenever I needed. A huge thank you goes to Dr. Barry Hirsch and Seth Mcafee that helped me with their medical knowledge, inviting me to the OR and being so patient during all trials. Thanks also to Linda Phillips, form OmniGuide, who gave me support sending and providing all the necessary material regarding the laser.

Second, a super huge thanks to my family for supporting me for all these months, being my “sponsor” and giving me the possibility to live this awesome experience.

Third, a special thanks to all my friends in Pittsburgh (Giorgio, Fernando, Cristian, Nicola and Simone) that made my “American experience” so special.

Table of Contents

1 INTRODUCTION 1

1.1 Purpose and objectives 2

2 MEDICAL BACKGROUND 3

2.1 Anatomy of the ear 3

2.2 Otosclerosis 6

2.3 Stapedotomy 7
2.3.1 Surgical procedure 8
2.3.2 Surgical requirements and robotic approach 10

3 STATE OF THE ART 11

3.1 Taxonomy of surgical robotic systems 11
3.1.1 Master/slave robots 11
3.1.2 Cooperative robots 14
3.1.3 Handheld robots 15

3.2 Comparison 19

4 MICRON: A HAND TREMOR CANCELLING INSTRUMENT 21

4.1 Hand tremor: a brief introduction 21

4.2 Micron hardware and software 22

4.3 Micron control 26
4.3.1 Micron frame systems 26
4.3.2 Micron and human feedback loop 27
4.3.3 Goal position filter 29

4.3.4 Micron controller 30
4.3.5 Micron control loop 33

5 MATERIALS AND METHODS 35

5.1 Ear model 35

5.2 Tools design and manufacturing 37
5.2.1 Requirements 37
5.2.2 Design and manufacturing process 38
5.2.3 Workspace analysis 42

5.3 Brace design 47

5.4 Handle design 48

5.5 Control tuning and calibration 49
5.5.1 Calibrations 49
5.5.2 System identification 50

6 EXPERIMENTS 59

6.1 Experiment configurations 59

6.2 Experiment steps 61
6.2.1 Bone trials 61
6.2.2 Model trials 64

6.3 Measured variables 64
6.3.1 Image Processing and Measures 65
6.3.2 Depth measure 70

7 RESULTS 75

7.1 Rosette geometrical data 75

7.2 Tremor reduction 79
7.2.1 Tremor cancellation effect 81

7.3 Depth penetration measure 82

7.4 Rosette completion time 84

7.5 Statistical Analysis 85

8 DISCUSSION 89

8.1 Surgeons' opinion 92

8.2 Future improvements 94

9 CONCLUSION 97

10 RIEPILOGO E CONCLUSIONI *(IN ITALIANO)* 99

11 BIBLIOGRAPHY 111

List of Figures

Fig. 2.1: Structure of the human ear. (http://ykia.gr/καταδυτική-ιατρική/, 2015.01.29). 3

Fig. 2.2: Middle ear ossicles: malleus, incus and stapes. They connect the tympanic membrane to the inner ear. (http://healthfavo.com/inner-ear-bones.html, 2014.11.5). 4

Fig. 2.3: Lateral view of the stapes [7]. Footplate (flat base) and superstructure (curura) can be seen. 5

Fig. 2.4: Different locations of otosclerosis (http://medical-dictionary.thefreedictionary.com/otosclerosis, 2014.11.6). 6

Fig. 2.5: Performing the rosette with laser [10]. 9

Fig. 2.6: After the rosette is performed on the stapes footplate the piston-prosthesis is placed [10]. 9

Fig. 3.1: Da Vinci® Surgical System, Intutitve Surgical (http://intuitivesurgical.com/company/media/images/davinci_standard_images.html, 2014.11.15) 12

Fig. 3.2: Surgeon using RobOtol (left) and front view of RobOtol (right)[9]. .. 13

Fig. 3.3: MMS-II manipulator and controller (left) showed in a typical surgical environment (right) [10]. 13

Fig. 3.4: Steady-hand robot by Johns Hopkins University [12]. 14

Fig. 3.5: Micron, 3-DOF: hand piece (left) and rendering of the active part (right) [15]. 17

Fig. 3.6: 6-DOF Micron (left), 6-DOF manipulator (right) [24]. 17

Fig. 3.7: ITrem hand piece [25]. 17

Fig. 3.8: Hand piece of AID (left) and IPCM actuator (right) [27]. 18

Fig. 3.9: High precision device using a linear delta manipulator [23]. 18

Fig. 3.10: SMART [28]. 19

Fig. 4.1: Human hand motion [15] (time domain): high frequency tremor, wander and jerk are shown. 22

Fig. 4.2: Micron system components: hand piece, electronics and PSD cameras (part of the ASAP apparatus). 23

Fig. 4.3: Micron handpiece head: active part. 24

Fig. 4.4: Micron UI made with LabVIEW. With this UI the user can control Micron. 25

Fig. 4.5: Micron coordinate systems. 27

Fig. 4.6: Feedback loop considering an operator holding a handheld active instrument [15]. The handheld active instrument is represented by the G_A Aid dynamics block. 28

Fig. 4.7: Control loop showing in particular the action of the aid dynamics G_A (handheld active instrument: Micron) [15]. 28

Fig. 4.8: H(s) goal position filter: scaling and low-pass filters [15]. f_L and f_H are the corner frequencies of the scaling filter and k_s is the amplitude of the scaling filter. 30

Fig. 4.9: Micron IMC architecture controller. 31

Fig. 4.10: IMC modified architecture, possible when $Q = G - 1$. 31

Fig. 4.11: Response of the tip lateral motion to a step of the handle. The step was injected numerically from Micron UI. Plots of system model behavior (blue) and adding the controller (red). The model and the controller were the result of system identification process. 32

Fig. 4.12: Micron control loop considering kinematics and position vectors [15]. 33

Fig. 5.1: Ear model: dimensions of the ear internal workspace, with maximized dimensions [13]. The internal workspace was approximated to a truncated cone and a cylinder. 36

Fig. 5.2: Ear model made with speculum, plastic tube to simulate the ear canal, and a target on the bottom inside the clay layer (left); and the view from the microscope, where the target can be seen (right). 36

Fig. 5.3: Middle ear surgical instruments hook on the tip. 38

Fig. 5.4: Bend-shaped surgical tool for ear surgery. 39

Fig. 5.5: Bayonet-shaped surgical tool used in stapedotomy. 39

Fig. 5.6: Mockup of the one-bend-shaped tool. 39

Fig. 5.7: Mockup of the bayonet-shape tool. 40

Fig. 4.8: Tool tip (fenestraiting pick) assembly: bayonet-shape, connector and tip. 40

Fig. 5.9: Laser tool for Micron. 41

Fig. 5.10: Initial configuration and reference frame of Micron. The P_i points are the vertexes of the moving plate; the F_i are the points that connect the flexures and the stacks and B_i are the base points. The green patch is the moving plate; instead the cyan one is the fix base. 43

Fig. 5.11: Initial pose: bayonet-shaped tool configuration. The bayonet is modeled as two segments, but the important point is the tool tip (T tip). 43

Fig. 5.12: Bayonet-shaped tool configuration workspace. The shape of the workspace is a squashed cube that can be seen in the xy-plane (left) and in 3D space (right). 47

Fig. 5.13: Micron with the old plastic white handle. The tip and brace where initial prototypes. 48

Fig. 5.14: Previous plastic handle. 48

Fig. 5.15: Micron handpiece with the new re-designed handle. 48

Fig. 5.16: Black box model for system identification. 51

Fig. 5.17: Stimulus: sweep sine input signal. Frequency range: 5-1000 Hz. The length of the input signal was 10 s. 52

Fig. 5.18: Tip (left) and laser (right) tool frequency response. 54

Fig. 5.19: xy (left) and z (right) frequency response, model and reduced model comparison, for the fenestrating pic. 55

Fig. 5.20: xy (left) and z (right) frequency response, model and reduced model comparison, laser probe. 55

Fig. 5.21: Tip xy (left) and z (right) reduced model and controller frequency response (Bode plot). 56

Fig. 5.22: Laser probe xy (left) and z (right) reduced model and controller frequency response (Bode plot). 57

Fig. 6.1: Temporal bone (left), and its location (right) in the human skull [http://wellnessadvocate.com/?dgl=10232, 2014.12.6]. The round hole in the center of the temporal bone is the ear canal. 60

Fig. 6.2: Temporal bone holder (left) and experiment configuration with temporal bone holder, speculum, speculum holder and hand rest (right). 62

Fig. 6.3: Experiments setup. All the components can be seen: 1) Micron, 2) target (bone in this case) and bone holder, 3) speculum, 4) speculum holder, 5) ASAP, 6) microscope, 7) laser machine, 8) hand rest. 62

Fig. 6.4: Graphical User Interface developed for image processing of the photos taken to the rosettes after each trial. Image is first processed, and than some geometrical parameters are computed. Superimposed to the bottom black and white image, the green line is the rosette contour detected, the red line is the equivalent circle, the blue line the best ellipse fit, the yellow dotted line the ideal rosette and the red points are the centroid and the supposed center of the rosette. 66

Fig. 6.5: Rosette contour detection and calculus of the RMS error, index of the irregularity of the rosette contour. 67

Fig. 6.6: Tip trajectory in the space while performing the rosette using the laser. 68

Fig. 6.7: Rosette contour detection (green), best fit ellipse (blue), equivalent area circle (red) and ideal rosette shape (yellow). This is the result of image analysis of bone trials. 69

Fig. 6.8: Scans of the tip trajectory during the procedure to compute the normal vector to the stapes footplate surface. The normal vector **n** is in magenta. The three scans are as vertical as possible, but the reference system is the ASAP, so they appear with some angle according to the ASAP pose during the trial. 72

Fig. 6.9: Distance point - plane. 73

Fig. 7.1: Rosette performed during a model trial: the ear model was used as target. It can be seen the yellow shape that resembles the stapes footplate shape and the black rosette in the center performed by overlapping laser bursts. 75

Fig. 7.2: Bone fenestrations, surgeon 1 (left) and surgeon 2 (right). 77

Fig. 7.3: Tremor cancellation effect: cancellation off (unaided case) (left) and cancellation on (aided case) (right). The wanted motion (green) is the actual motion (blue) minus the tremor (red). 79

Fig. 7.4: Hand, goal and tip position comparison unaided (left) versus aided (right) case. 81

Fig. 7.5: 2D trajectory while performing the rosette comparison: unaided (left) versus aided (right). 82

Fig. 7.6: Mean Z depth penetration during bone trials. σ is reported as a vertical line for each bar. 83

Fig. 7.7: Geometrical data of all the trials: mean e (left) and $RMS_{contour}$ (right). σ is reported as a vertical line for each bar. 86

Fig. 7.8: Tremor data of all the trials: RMS_{tremor} (left) and Max_{tremor} (right). σ is reported as a vertical line for each bar. 86

List of Tables

Table 2.1: Average and range of stapes dimensions. This table is referred to Fig. 2.3 [7]. 5

Table 3.1: Comparison of feature for different robot types [15]..... 20

Table 4.1: Cancellation filter parameters [15]. 30

Table 6.1: Model trials order: succession of aided (On) and unaided (Off) case. 60

Table 6.2: Bone trials order: succession of aided (On) and unaided (Off) case. 60

Table 6.3: Ideal rosette data: this is a circle with 800 μm diameter..... 70

Table 7.1: Surgeon 1, rosettes geometrical results comparison in model trials: unaided vs. aided case. 76

Table 7.2: Surgeon 2, rosette geometrical results comparison in model trials: unaided vs. aided. 77

Table 7.3: Surgeon 1, bone trials rosette geometrical results comparison: unaided versus aided. 78

Table 7.4: Surgeon 2, bone trials rosette geometrical results comparison: unaided versus aided. 78

Table 7.5: RMS_{tremor} and Max_{tremor} displacement of the tremor during the rosette task in model trials. 80

Table 7.6: RMS_{tremor} and Max_{tremor} displacement of the tremor during the rosette task in bone trials. 80

Table 7.7: Depth penetration results in bone trials. The zero-plane and the error are defined in chapter 6.3.2. 82

Table 7.8: Model trials rosette completion time. 84

Table 7.9: Eccentricity and $RMS_{contour}$ computed grouping all the trials. 85

Table 7.10: RMS_{tremor} and Max_{tremor} computed grouping all the trials. 86

Table 7.11: *p*-values from the nonparametric statistical KS and KW tests: the statistical significance between Micron on and off was tested. The significance level was 0,05. 87

Abstract

Robotic-assisted surgery is a rapid growing field, facing challenging tasks and demands from surgeons, in particular in minimally invasive and microsurgery. However many of the present robotic systems are not well integrated in the surgical workflow, too big or too expensive. Micron is an innovative fully handheld active micromanipulator that helps surgeons to improve position accuracy and precision in microsurgery by cancelling the hand tremor. This thesis describes adaption, tuning and testing of the Micron for stapedotomy, microsurgical procedure performed in the middle ear to restore hearing. This procedure requires accurate manipulation in narrow spaces as the ear canal and middle ear. Two end-effectors, a handle and a brace or rest were designed and prototyped and the control system was adapted for the new hardware; the system was tested in stapedotomy procedure *ex-vivo*. Tremor amplitude was found to be reduced significantly. Further testing is needed in order to obtain statistically significant results regarding other parameters dealing with regularity of fenestra shape.

Key words: microsurgery, ear surgery, hand tremor, tremor cancellation, surgical robotics.

Sommario *(in italiano)*

La chirurgia robotica è un campo in rapida espansione, che fa fronte a sempre maggiori sfide tecnologiche e richieste da parte dei chirurghi, soprattutto nella chirurgia mini-invasiva e microchirurgia. Tuttavia molti dei sistemi robotici per non sono ben integrati nel processo chirurgico, di dimensioni elevate o con un costo troppo oneroso. “Micron” è uno strumento attivo usato per la micro-chirurgia. Il chirurgo usa Micron come fosse uno strumento convenzionale, ma che, con un approccio innovativo, cancella il tremore, aumentando così la precisione durante la manipolazione. Questa tesi propone uno sviluppo e adattamento di Micron all’operazione di stapedotomia, intervento

microchirurgico all'orecchio medio avente lo scopo di risolvere problemi d'udito (otosclerosi). In questo scenario è richiesta un'elevata precisione di manipolazione in spazi ristretti, come il canale auricolare e l'orecchio medio. Due strumenti, un'impugnatura e una protezione sono stati progettati e sviluppati e i parametri di controllo adeguati; alla fine le prestazioni con Micron-on (attivo) sono state valutate mediante esperimenti e comparate con quelle con Micron-off (disattivo, simile a uno strumento chirurgico tradizionale). Promettenti risultati sono stati ottenuti nella cancellazione del tremore e riduzione dell'oscillazione ma ulteriore sperimentazione è necessaria per capire l'effetto di altri parametri che influenzano il risultato nel caso di Micron attivo.

Parole chiave: microchirurgia, otologia, tremore, cancellazione del tremore, robotica chirurgica.

1 Introduction

This thesis work is centered on Micron, a fully handheld instrument that aims to help otologic surgeons to improve the outcomes of middle ear surgery with the achievement of high positioning precision and accuracy through hand tremor[1] suppression.

Middle ear microsurgery is particularly challenging since surgeons have to manipulate human body parts about few hundred microns, and visualizing the surgical area through a microscope [1]. Moreover middle ear surgery is minimally invasive, not an open surgery: it is performed in an internal cavity, the middle ear, accessed trough the ear canal. This fact makes these procedures even more challenging due to the limited space of motion. Another challenge derives from the reduced visibility: such conditions are at the "limit of human perception and dexterity" [2].

Technology can help surgeons in these challenging operations: robot-aided surgery offers a multiplicity of advantages. Thus, surgeons' operative skills are enhanced during these delicate procedures. Robotic systems allow achieving better positioning precision and accuracy, high dexterity, motion scaling and tremor filtering.

Nowadays the most common surgical robotics systems are the master/slave systems in which there is a mechanically grounded robotic arm with multiple links and a console to control the robot. These systems have several advantages, like tremor filtering, motion scaling and remote control, but they are also complex, bulky, expensive and completely change the traditional surgical workflow [3].

To overcome these drawbacks, the novel approach of handheld robot called "Micron" was first proposes at Carnegie Mellon University by Riviere et al [4], in order to cancel hand tremor so that the tool mounted on the robot is extremely

[1] [1]Tremor: shaking of the hand in high frequency. It is an involuntary motion, but natural. Further explanation will be given in chapter 4.1.

stable and not affected by unwanted tremor motion, enhancing positioning accuracy and precision during microsurgery.

Handheld robots have the advantage of being inexpensive, if compared with the other surgical robotic systems, easily integrated in the conventional surgical workflow since they are small and similar to a surgical instrument. They enhance the skill of the surgeon since they are handheld and they are safe, because if the system fails, the removal from the surgical area is safe and easy and the surgery can be completed with conventional tools [3].

1.1 Purpose and objectives

This thesis work aims to develop instruments and means to adapt Micron for middle ear surgery and test and assess the performance of the system in real surgical conditions.

Firstly some tools were developed: a fenestrating pick and a laser probe were designed and manufactured. Then Micron control system was tuned for the new tools and the control parameters set to obtain an optimal tremor cancellation. The final step was the simulation of real surgical conditions. Initially experiments were done using an ear model and successively using some cadavers' temporal bones, to be as close as possible to the real surgical settings.

At the end experiment data analysis helped to understand the effect of Micron and compare the results in the robotic aided and unaided case.

2 Medical background

This chapter gives all the necessary information to understand the medical procedure taken as target for this thesis work: starting form the anatomy and moving to the causes of the disease, and finally describing step by step the surgical procedure.

2.1 Anatomy of the ear

The anatomy of the human ear is described thoroughly in [5].

The ear is part of the auditory system and is the organ that allows us to detect the sound, but it is also important for balance. The ear is divided conventionally in three parts: outer ear, middle ear and inner ear (Fig. 2.1).

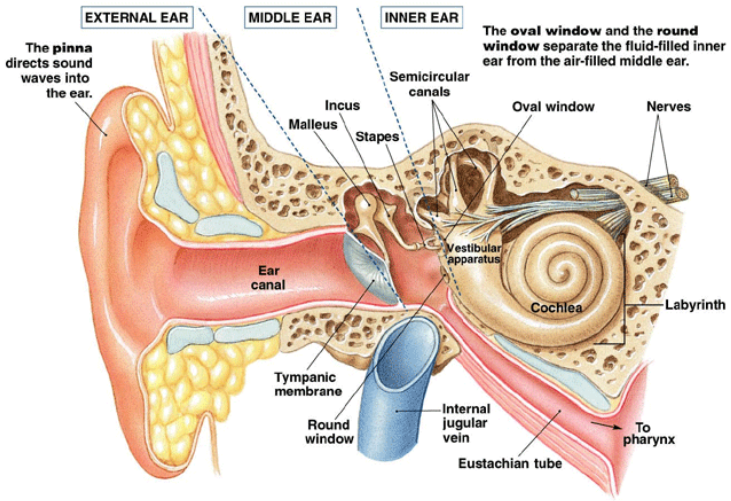

Fig. 2.1: Structure of the human ear. (http://ykia.gr/καταδυτική-ιατρική/, 2015.01.29).

Through the ear canal the eardrum (or tympanic membrane) can be reached. It is the beginning of the middle ear. The external ear conveys the sound waves from the outside to the tympanic membrane. The impact between sound waves and the eardrum cause it to vibrate.

The middle ear includes the three auditory bones (ossicles): the malleus (or hummer), the incus (or anvil) and the stapes (or stirrup) (Fig. 2.2). The malleus is connected to the tympanic membrane and the stapes is connected to the oval window over the vestibule, part of the cochlea. The incus is a bridge that connects the malleus and the stapes. The stapes footplate lies on and pushes the oval window, and this motion causes motion of the fluid within the vestibular apparatus (Fig. 2.1).

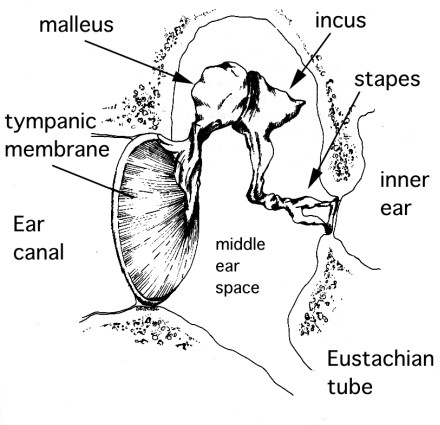

Fig. 2.2: Middle ear ossicles: malleus, incus and stapes. They connect the tympanic membrane to the inner ear. (http://healthfavo.com/inner-ear-bones.html, 2014.11.5).

The sound waves are transmitted in form of vibrations, form the eardrum to the malleus, through the incus to the stapes, and from the footplate of the stapes to the oval window. So the three ossicles form a sort of vibrating transmission chain, which amplifies the vibration: this because the malleus-incus complex acts as a lever about its rotational axis, giving a mechanical gain [6].

The inner ear contains the cochlea, the sensory organ for hearing and the organs for motion and balance. These are respectively the vestibular apparatus and the semicircular canals. The fluids movements inside the cochlea are transmitted to

the vestibulochoclear nerve (auditory nerve), which finally transmit impulses to the brain, where the impulse is classified as sound.

The most interesting bone for the purposes of this thesis is stapes (Fig. 2.3). It was studied scrupulously in [7]. The name comes from its particular stirrup-like shape: in fact, "stapes" in Latin means stirrup. It is formed by a base (footplate) and a superstructure (two curura).

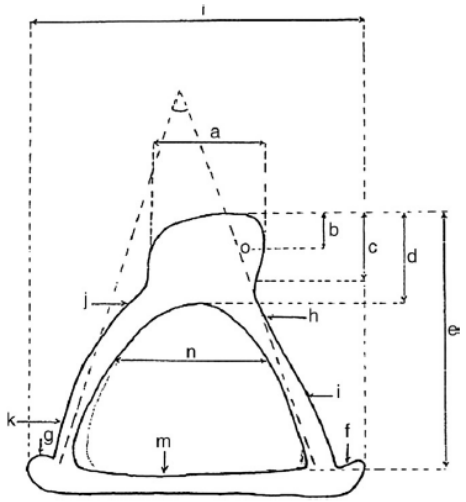

Fig. 2.3: Lateral view of the stapes [7]. Footplate (flat base) and superstructure (curura) can be seen.

In Table 2.1 some important dimensions are reported to have a clear understanding about the physical dimensions of the smallest and lightest bone of the human body.

The following numbers were measured out of 12 stapes, form male patients with average age of 50-years. An electronic microscope was used (accuracy: 1 μm).

(μm)	m	i	k	e	l
Mean	228	251	191	2612	2298
Range	178-338	214-350	142-300	1892-3400	1928-3050

Table 2.1: Average and range of stapes dimensions. This table is referred to Fig. 2.3 [7].

Only relevant quantities for this thesis work are reported in Table 2.1, for further information please refer to [7].

2.2 Otosclerosis

Otosclerosis affects circa 10% of the population [8]. This high percentage means also high costs for the sanitary system.

Hearing loss can be divided in two types: conductive and sensorineural. This distinction is essential, because only the conductive hearing loss can be corrected by surgery [6].

Otosclerosis is a hearing impairment of the ear due to abnormal and excessive bone growth. This interferes with the normal vibration of the middle ear bones, in particular the stapes, which is the final link in the transmission chain (Fig. 2.4).

Anything that interferes with the stapes and its motion results in hearing impairment: it creates bone entrapment that obstructs proper sound transmission to the inner ear [9].

The causes of otosclerosis are still unknown, however there are some researches that state that it is a hereditary disease [6]. Others think that otosclerosis is due to immunologic reaction. Modern genetic support both the theories [10].

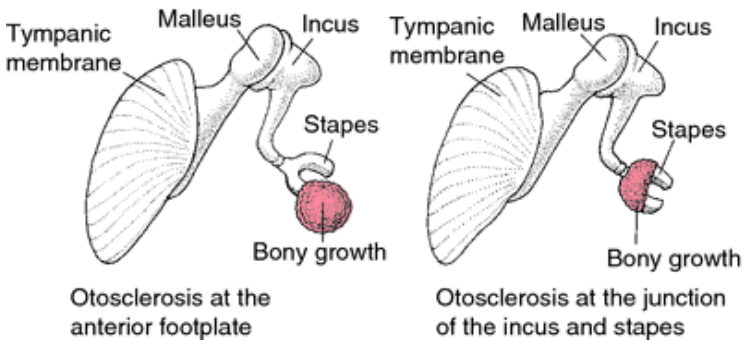

Fig. 2.4: Different locations of otosclerosis (http://medical-dictionary.thefreedictionary.com/otosclerosis, 2014.11.6).

In the early stage of the disease hearing aids can be helpful, but with its progression, surgery is needed: the surgical procedures are called stapedectomy and stapedotomy. These two operations are similar but this thesis work refers to the latter (see next chapter).

2.3 Stapedotomy

Stapedotmoy is a surgical operation of the middle ear that aims to cure the stapes fixation and replace the hearing sense totally or partially.

The reasons for the stapes fixation is most commonly otosclerosis, but in some cases congenital malformation of the stapes can happen, but this disease is far less common; so the focus will be mainly on otosclerosis.

Today the results of this operation are, in the majority of the cases, successful. This is due to a well-defined procedure, with specified and well optimized steps [10] [11].

Stapedotmoy consists in the replacement of the immobile stapes with prosthesis. This surgical procedure is really delicate and requires precise manipulation because erroneous contacts can lead to complications and malfunctioning of the ear apparatus after the surgery.

The middle ear bones have the function of amplifying the vibration. This bony chain has to move freely for an optimal sound transmission and amplification.

The surgical solutions to cure otosclerosis are stapedectomy or stapedotomy. There is a small difference between these two procedures. According to the American Academy for Audiology, “A limited opening/hole within the central footplate of the stapes (accomplished via laser or manually with a drill) is referred to as "stapedotomy." Total or subtotal removal of the stapes footplate (usually accomplished manually) is referred to as "stapedectomy" “ [12].

Stapedotomy is a surgery that has been performed for over 52 years. During this long period, improvement of the process and instrumentation were made. The two most important developments to obtain a better outcome were the Teflon cup piston prosthesis and the fiber-optic laser [11].

The rate of success of stapedotomy is over 95%. This percentage decreases over time, but this is due to the ageing process and further effects of otosclerosis [11]. But overall, stapedotomy is, in the majority of the cases, a successful operation.

2.3.1 Surgical procedure

This surgical procedure is described thoroughly in [10].

To perform stapedotomy, the patient is premedicated by nurses and the ear is prepared to the surgery, which is performed under anesthesia. The patient is placed with the chin towards the shoulder, in a way that the ear to be operated is well positioned (ear up).

The first phase is the ear canal incision performed with a tip-rounded knife close to the eardrum. The eardrum is lifted up, so there is access to the ossicles. A speculum (funnel shape metal part) is placed and fixed with a holder. The speculum is useful for the surgeon as it serves as a base to pose tools and keep the access open, so both the hands are free.

The mucosa around the ossicles is anesthetized, and the malleus and incus are controlled. If the visibility of the stapes is insufficient, part of the scutum (bone in the ear canal) is removed using a curette (surgical instrument that is a sort of small cutting spoon).

At this point the stapes is clearly visible, and the stapes fixation is verified. Also the stapes footplate is checked. The surgeon than examine the footplate to find out the best point for the perforation. The joint between the stapes and the incus is divided and the stapedial tendon is cut.

For the next steps of the procedure two approaches can be used: using manual techniques or the laser. Only the laser technique is described here, since it is the most used.

Using the *laser* the anterior and the posterior crus of the stapes are cut. After that the superstructure of the footplate is removed. Now the footplate is exposed completely. At this point, using the laser, a rosette-shape (fenestra) is created on the footplate: this is done by overlapping every burst until a round shape is created (Fig. 2.5). The ideal fenestra is a circle of 800 μm in diameter.

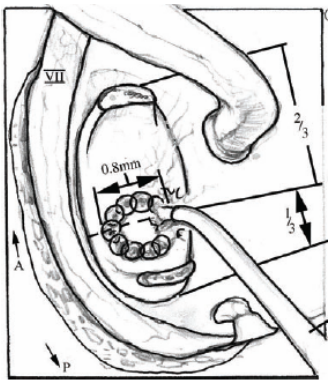

Fig. 2.5: Performing the rosette with laser [10].

Then the bony fragments inside the fenstra are taken out using a sharp pick (*fenestrating pick*) and the edge of the rosette is smoothened; then the piston prosthesis is placed.

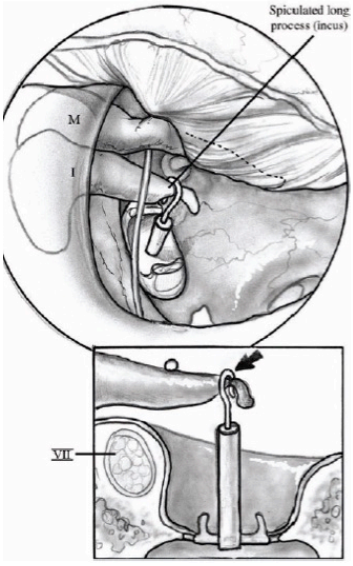

Fig. 2.6: After the rosette is performed on the stapes footplate the piston-prosthesis is placed [10].

This prosthesis is piston-shaped, with an open ring at the top that has to be fixed on the incus. The distance between the incus and the stapes footplate is quite constant [10]. At this point the prosthesis is in place and the ring is tightened: this procedure is delicate since if the ring is too tight, necrosis (death of the

tissue) occurs, and if the ring is too loose it will be worn out by the incus motion. Finally the ring is verified by instrument palpation.

The last step is to put the tympanic membrane back in place. Then antibiotic ointment is shed in the ear canal. After that, the operation is finished and the patient can return to the recovery room.

2.3.2 Surgical requirements and robotic approach

Stapedotomy is a middle ear surgery that involves the smallest bone of the human body, requiring highly accurate gestures; thus robotic-aided procedures have the potential to enhance the outcome of this surgery.

Main difficulties of the stapedotomy procedure are [13]:

- Keyhole surgery, i.e. the procedure is performed through a hole of the human body. This fact leads to efforts due to the narrow and confined space to reach and operate on the target area;
- The use of the microscope: the vision is the main feedback that surgeons have. Because of the narrow spaces, sometimes the surgeon's hand and the tool can obstruct the visual field;
- Structures involved in stapedotomy are small and fragile, so the forces are tiny: because of this tactile feedback is not quite useful.

In particular, there are two phases of stapedotomy that requires more precision that the others. These are the crimping of the piston prosthesis on the incus and performing the fenestration on the stapes footplate [14]. Here the focus is on the latter.

Since the fenestra size should be 800 μm in diameter, great accuracy is required. The robotic technology can be for sure helpful to enhance the positioning precision and accuracy.

The more controlled motion is important also to avoid touching and hurting delicate parts of the middle ear.

3 State of the Art

Many surgical robotic devices have been developed in the past few years, for a wide range of specific surgical operations, with different accuracy, dimension, complexity and cost.

In this work the attention is focused on robots used in ear surgery, since this is the goal. So an overview on different types of robots is done but the attention is mainly paid for the ear robotics.

According to [15] and [16] the taxonomy of robots used in microsurgery includes the following categories:

- Master/slave robots
- Cooperative robots
- Handheld robots

In the following chapters these types are described and compared.

3.1 Taxonomy of surgical robotic systems

In this chapter a classification of different robotic systems is presented, highlighting the characteristics and corresponding pros and cons.

3.1.1 Master/slave robots

A master/slave system (or teleoperated system) consists of two separate subsystems: the console, where the input from the user is given (master) and the system that actuates the end effector (slave). There is no direct mechanical connection between master and slave, but only electrical. Through the software, filters can be applied as well as scaling motion: so the workspace is not limited

by the range of motion of the user, but can be larger or smaller, depending on the scaling factor used.

An example of a master/slave system is the da Vinci® system (Fig. 3.1), by Intuitive Surgical [17]. This robot has many applications in different types of surgery, including what is called ENT (ear nose and throat) surgery. Up to now there are no surgeries at the middle ear using this robot [18]. This because middle ear surgery has an internal surgical site that is extremely small. The access point is only one, the ear canal: this represents a problem for the use of this system due to the dimensions of its robotic arms.

Miniaturization of instruments is required for master/slave robots in order to grow in the area of otology [18].

Fig. 3.1: Da Vinci® Surgical System, Intutitve Surgical
(http://intuitivesurgical.com/company/media/images/davinci_standard_images.html, 2014.11.15)

Miroir et al [13][19] in 2012 studied the characteristics of the middle ear surgery, its dimensions and microsurgical gestures in order to design a teleoperated assistance robotic system, called robOtol. They focalized on the middle ear procedures, since those are the most complicated and delicate procedures.

RobOtol (Fig. 3.2) has 6-DOF (degrees of freedom). It is remotely guided with a robot-surgeon interface.

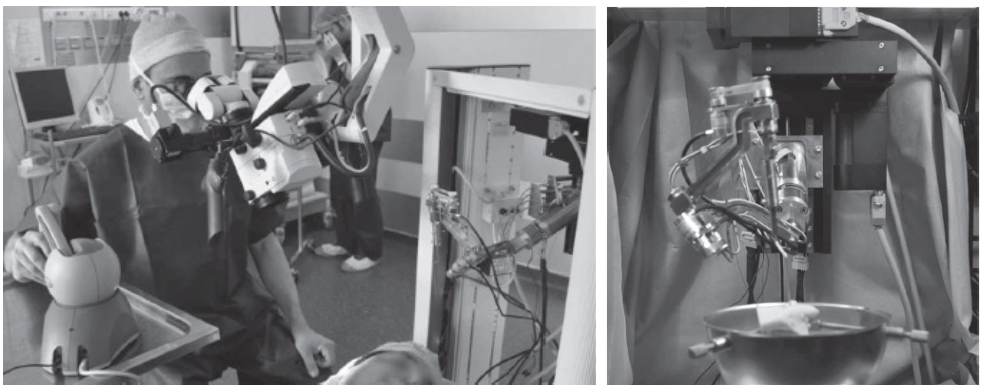

Fig. 3.2: Surgeon using RobOtol (left) and front view of RobOtol (right)[9].

Another master/slave robot developed by Maier et al is MMS-II robot [20] (Fig. 3.3). MMS-II has 4-DOF, XYZ and a rotation of the end effector. It is controlled by a console with two joysticks.

A characteristic feature of MMS-II is its size: it is small enough to be clamped at the operating table, with the console in front of the surgeon that looks into the operating microscope. So it does not require a big space, like the da Vinci®.

Fig. 3.3: MMS-II manipulator and controller (left) showed in a typical surgical environment (right) [10].

Master/slave systems (and in particular the Da Vinci) are the most spread among surgical robots, but their use is still constrained to US and Europe, due to the high initial cost, the high cost of maintenance and set up [3].

3.1.2 Cooperative robots

In cooperative robots the control is mutually divided between the user and the robot, so cooperation is created between the surgeon and the robot. The same tool is held by the user and attached to the robot, so the robot senses the force and movements applied by the user to the instrument and also the reaction forces from the environment. These data are then used, through a controller, to enhance user performances by cancelling tremor, scaling force and augment accuracy.

Steady-hand robotic system [21] (Fig. 3.4) have been developed at Johns Hopkins University with the following intent: “Our goal is to develop a manipulation system with the precision an sensitivity of a machine, but with the manipulative transparency and immediacy of hand-held tools”.

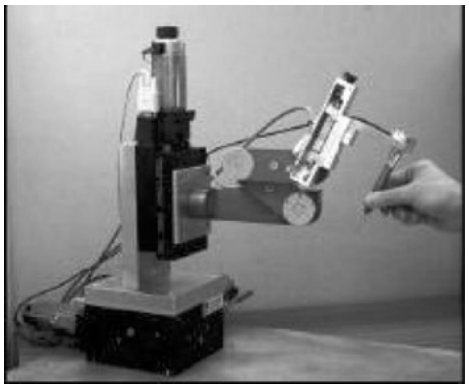

Fig. 3.4: Steady-hand robot by Johns Hopkins University [12].

Steady-hand robot was at first developed for eye surgery, but further developments are in the field of neurosurgery, microvascular and ENT surgery. In particular some trials were done performing stapedectomy [14].

If compared with the master/slave robots, the cooperative have the following advantages:

- Simplicity of the system;
- They are cheaper;
- The surgeon holds directly the instrument, so the approach is more direct and intuitive. For this reason surgeons are more inclined to accept a cooperative then a master/slave approach.

However they lack certain aspects, like the possibility of scale the motion. Moreover, in cooperative robots, tremor can be suppressed but the human hand tactile feeling is lost. Recent development is the force sensing through some sensors mounted on the end effector that allows having force feedback to the user [22].

3.1.3 Handheld robots

Handheld micromanipulators are a fairly new concept. The primary focus of this thesis is on these devices. A complete review of hand-held manipulators is done in [3].

These robots have the actuation system on the hand piece, there is no robot arm involved, so they are not grounded, and the surgeon holds the active tool as a conventional surgical tool.

The advantages of such systems are [3], [15]:

- "Hands on" approach: the surgeon has total control over the tool since the tool is on his hands and not control remotely;

- Dimensions: they do not require large space in the OR;

- Safety: in case of system failure, since the active instrument is hand-held, it is easy to remove from the surgical site, and continue the procedure with conventional tools;

- Workflow close to normal procedure: since the surgeon himself holds the instrument, there is no big difference from a conventional surgical workflow;

- Reduced cost: since the system is not so complex as the other types of robots, the initial cost is lower. Moreover these systems do not require elaborate set-ups, so also the cost related to the time use of the OR (operating room) is reduced.

Challenges of implementation of hand-held systems are [3], [15]:

- Miniaturization: the handle dimension should be close to a conventional surgical tool, and the mass has to be reduced as much

as possible. The actuator design is particularly challenging since those should be compact in size, light weight and have the maximum range of motion as possible;

- Hand piece weight and inertia: mass and inertia are two parameters to take particularly care of. Motors, sensing system and other electronics can increase the weight significantly, having the effect of augmenting the hand tremor rather than suppressing it. The objective is to keep the manipulator weight and inertia as low as possible;

- Avoid motion artifacts: motion artifacts can be generated form the reaction forces of the motors, since they are not supported by grounded base, but mounted on the handle;

- Control stability: the control loop has to be stable and capable of enough robustness;

- Sterility: since the active handle is close to biological tissue, it needs to be sterile. This can be a problem because the handle contains electrical instrumentation as actuators and sensors.

Since motors are present on the device, they are classified as active cancelling tremor systems. Passive system had been tried to cancel tremor too, but without success [23]. These systems act only like a low pass filter, without fully eliminating the hand tremor.

The first development of a cancelling tremor hand-held active instrument happened at Carnegie Mellon University (CMU), by Riviere et al, where in 2003 the first Micron was presented. In chapter 4, there is a detailed description of this device, since it was part of this thesis work.

After 2003, many developments and improvements followed, since nowadays two versions of Micron are used: a 3-DOF configuration mainly used for ear surgery (Fig. 3.5), and a further development that has 6-DOF, mainly used for eye surgery (Fig. 3.6). This thesis is focusing on the 3-DOF version, since the aim of this work is satpedotomy, a middle ear procedure. The 3-DOF is preferred for ear surgery because it is more robust, it can generate higher forces and its stability is superior compared to the 6-DOF.

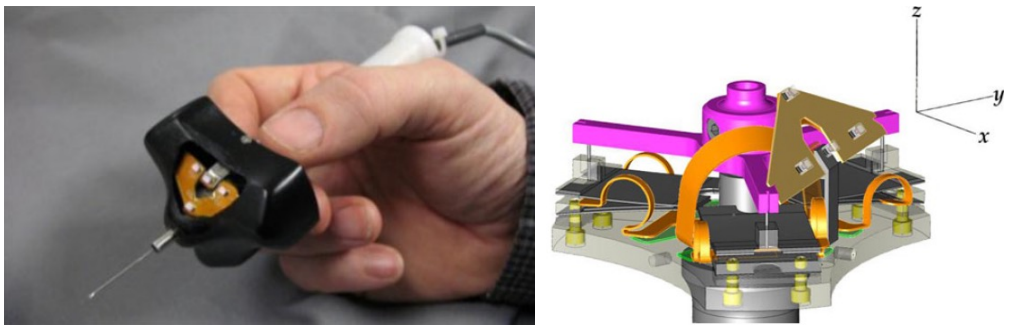

Fig. 3.5: Micron, 3-DOF: hand piece (left) and rendering of the active part (right) [15].

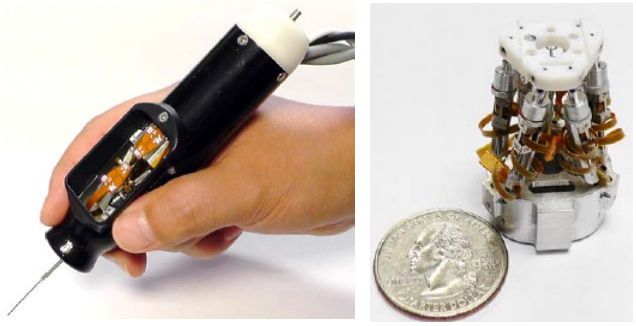

Fig. 3.6: 6-DOF Micron (left), 6-DOF manipulator (right) [24].

A "close relative" of 3-DOF Micron is ITrem, developed by Ang et al in 2009 [25] (Fig. 3.7). The functioning principles of this device are the same as Micron. There is a difference in the sensing subsystem that are implemented with inertial measurement units (IMUs) strategically positioned to achieve the maximum resolution of the position measure [26]. Another difference is the design of the manipulator subsystem, more compact and light.

Fig. 3.7: ITrem hand piece [25].

There were other trials to develop handheld manipulator by other researchers.

An interesting approach was presented in 2013 by Saxena et al [27]. This micromanipulator was called AID (accuracy improvement device): the tip in this instrument is actuated by an ionic polymeric metallic composite (IPCM). This allows the instrument to be really slim and light. The limitation here is the fact that the manipulator has only 1-DOF.

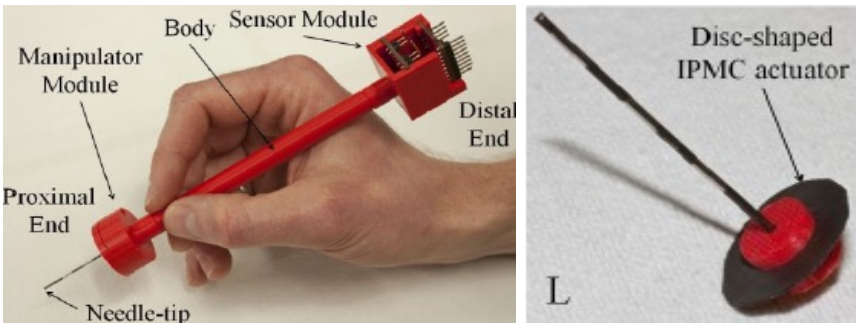

Fig. 3.8: Hand piece of AID (left) and IPCM actuator (right) [27].

In the same year, Chang et al proposed an instrument based on a linear delta manipulator [23] (Fig. 3.9). A linear delta manipulator is a device that provides high stiffness in the axial direction with a simple parallel structure. To actuate this structure 3 voice coil motors (VCMs) with 3 high resolution encoders were used. This manipulator has a fairly big workspace compared to the other handheld devices, but there is no detection of the end effector.

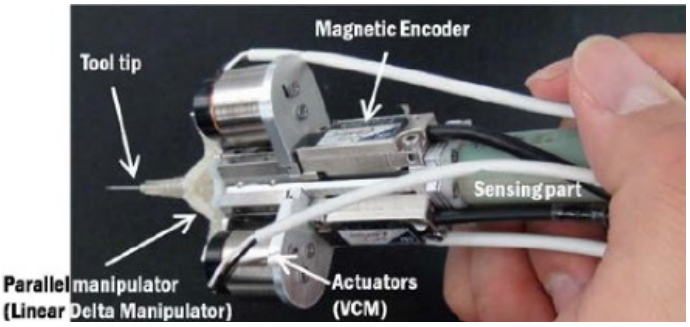

Fig. 3.9: High precision device using a linear delta manipulator [23].

Another interesting approach still in an early stage is the micromanipulator designed by Song at al [28] (Fig. 3.10). The interesting feature of this device is that it uses a piezoelectric motor coupled with an OCT (optical coherence tomography) sensor to achieve tremor cancellation and surface sensing. The OCT sensor allows measuring the distance between the needle tip and the target surface.

This system has only 1-DOF, but many advantages: slim conformation, cost effectiveness and the fact that the tip can easily be changed.

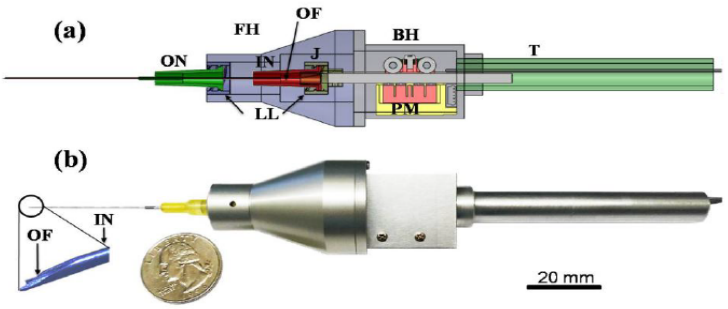

Fig. 3.10: SMART [28].

3.2 Comparison

Master/slave and cooperative robots have some advantage compared to handheld instruments. They can achieve a better accuracy and precision. Since they are fixed to the ground with a rigid structure, one arm can be left "in position" helping the surgeon to hold or grasp something; this is an advantage. They can also have a more ergonomic handle, since it does not have to house motors and sensors.

However they have some clear drawbacks: cost, big space required (sometimes and entire OR has to be dedicated) [29], long setup time [3] and lost natural sensibility.

Handheld robots have some key aspects that make them attractive: the cost is drastically reduced, the familiarity of the surgeon is kept since she/he is holding

an instrument close to the conventional ones and if failure of the system happens they are easily removable form the surgical site.

Riviere et al [15] did a comparison table, that is reported below (Table 3.1), where key aspects for a surgical robot are listed on rows and the different type of robots are in columns.

	Unaided	Master/Slave	Cooperative	Handheld
Motion scaling	No	Yes	No	Yes
Workspace intrusion	No	Slave arm and Master	Arm	Active tool, sensor sightlines
Force feedback	1:1	Research area	Yes (Superimposed on damping)	1:1
Set and forget hold	No	Yes	Yes	No
Features	Current practice	Could combine all of the above features, telemedicine	Inexpensive position-output actuators and simple control	Hand-held operation improves user acceptance and safety, mechanical simplicity
Challenges/Cost	Tremor limits accuracy and repeatability	Unproven force feedback performance / greatest mechanical and control complexity (high cost)	Dexterity fundamentally limited by force → rate user interface and low control bandwidth	Manipulator size and range, high bandwidth control / measurement subsystem cost

Table 3.1: Comparison of feature for different robot types [15].

4 Micron: a hand tremor cancelling instrument

This chapter gives an introduction and description of Micron, the active handheld instrument that is the main part of this thesis work. The chapter goes through a brief introduction of the human tremor, the early stages of Micron development and current solution available.

4.1 Hand tremor: a brief introduction

Before giving a picture of Micron, a brief explanation of the involuntary movement of the human hand in microsurgery is given, in order to understand its components and the reason why is important to get rid of it during microsurgery.

Involuntary hand motion is divided in 3 components (Fig. 4.1)[15]:

- Tremor: it is the high frequency component; the usual bandwidth is 8 – 12 Hz; it is defined as: involuntary, approximately rhythmic, and roughly sinusoidal movement [30], it is a normal component of hand motion in healthy people;
- Jerk: it is a sporadic fast movement of the hand;
- Wander: it is a slow trend motion of the hand away from the target point; it is a low frequency component.

These unwanted components have to be compensated by the micromanipulator to avoid tissues damage.

To obtain a precise and accurate motion in microsurgery it is necessary to get rid of all the three involuntary components, but preserve the voluntary motion. Voluntary (or wanted) motion is the actual motion minus the involuntary motion (high frequency tremor, jerk and wander):

Voluntary motion = Actual motion – Involuntary motion.

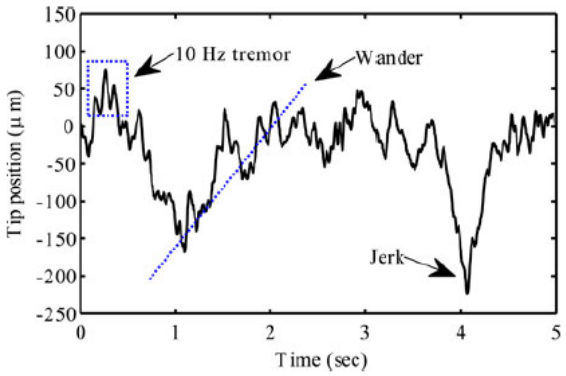

Fig. 4.1: Human hand motion [15] (time domain): high frequency tremor, wander and jerk are shown.

From now on, the involuntary movement is referred as tremor for straightforwardness: "any unwanted or involuntary motion of the hand" [31].

Tremor plays an important role in the outcome of microsurgeries: max errors in 3D are in the order of hundreds micrometers [31], the same magnitude order of the structure to manipulate.

Positioning accuracy of few microns can be reached only with robotic assistance [15]: this is the motivation of the development of Micron, an instrument that allows the surgeons to achieve better position accuracy for better surgical outcomes.

4.2 Micron hardware and software

In this chapter the description of Micron main components and its software is given.

The basic concept of Micron is that it compensates hand tremor by deflecting its tip in 3 DOF, with a motion equal but opposite to the hand tremor, so that compensation is accomplished.

The tip is actuated by three piezoelectric motors, thus Micron has three degrees of freedom (3-DOF). The tip can move in the plane (x, y directions) and axially

(z direction). In particular if stacks move all together, the tip motion is axial, instead lateral motion happens if opposed motors are actuated.

Fig. 4.2: Micron system components: hand piece, electronics and PSD cameras (part of the ASAP apparatus).

Micron system is made mainly by three hardware components (Fig. 4.2):

1. Micron (handpiece)

The handpiece, referred here as “Micron”, is composed of a handle, an active part and a tip (Fig. 4.3).

The handle is a hollow shaft hold by the user. Internally cables from the electronics components pass to reach the actuators.

The active part has a metal base where three piezoelectric stacks are attached: each actuator is made by two piezoelectric motors connected in series in a folded configuration. These actuators are mounted spaced of 120 degrees, to form a parallel configuration and their range of motion is 400 μm. To enhance the range of motion of these motors, flexure joints are present. There are 4 LEDs (Light Emitting Diodes, referred also as “lights”) that are detected by the PSD (position sensitive detection) cameras: 3 LEDs are attached to the actuated part called “spider” that holds the tip, and the remaining one is fixed to the base to detect the handle movement.

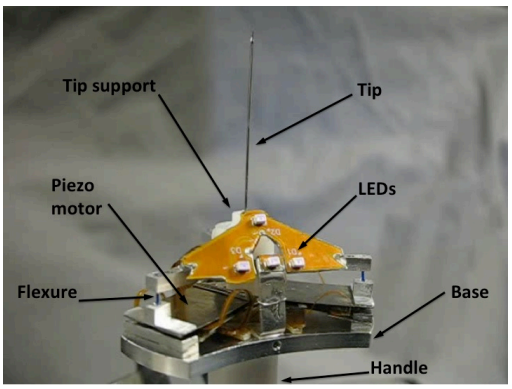

Fig. 4.3: Micron handpiece head: active part.

The actuated tip is the end effector of the system: different tools can be mounted according to the surgery needs.

2. Apparatus to Sense Accuracy of Position (ASAP)

The ASAP main components are 2 PSD cameras [32] (Fig. 4.2) and 4 infrared LEDs. This apparatus detects the tool position with a resolution of 4 μm at 2000 Hz; but an additional error is due to the fact that the tip has an offset respect the detected lights: this decreases the detection accuracy proportionally to the tool length [15].

The aim of the PSD cameras is to detect the position of the four lights: 3 placed on the tip and one placed on the handle. In this way the 6-DOF pose of the handle and the tip can be calculated in real time (see chapter 4.3.5).

Optical tracking methods are precise, but sometimes occlusion occurs between the receiver and the marker, leading at the failure [3]. However, other types of sensors, like inertial sensor, had been tried, but the optical tracking techniques are much more precise [3].

3. Electronics

The main electronic part is a machine that runs LabVIEW software in real time in which the control feedback loop is implemented. To control the parameters and have a general view on the process a GUI (guide user interface) is implemented in LabvIEW on a computer.

There is another component of the system: a foot-control having three different pedals. This component is not essential for Micron operations, but allows the user to switch Micron cancellation on and off, change the type of cancellation filter (see chapter 4.3.3) and trigger the recording of data.

The user, through a computer, controls Micron: the control loop parameters, setting, data collection, modes of operation and in general all that concerns control. This is done by some user interfaces (UI) developed in LabVIEW: different UI have been developed for different functions. The main one is called Micron UI, displayed in Fig. 4.4.

Fig. 4.4: Micron UI made with LabVIEW. With this UI the user can control Micron.

This UI allows the user to have a wide overview on Micron operations. The user can control: A) the motion of the stacks and if saturation occurs; B) if the

position of Micron handpiece is valid, that is when the PSD cameras can detect the LEDs; C) how data are recorded and displayed; D) if some stimulus is injected (used for testing Micron); E) pedals configuration; F) the displayed parameters; G) filters parameters; H) type of control; and I) which configuration to load (Fig. 4.4).

4.3 Micron control

This chapter describes Micron control loop, its filters and how cancellation functions. This helps to understand how Micron works and which operations are done every loop.

At first the coordinate systems are shown, then a feedback loop considering the influence of a hand-held robot on humans is presented.

The cancellation filter is described, being one of the most important filters of the loop, because it is responsible for the filtering of the hand motion, so which components are pass as voluntary motion and which others are filtered out like tremor.

The controller architecture and functioning is presented.

The last part describes the control loop as MIMO (multiple input multiple output) system.

4.3.1 Micron frame systems

Before describing the control loop it is useful to introduce the coordinate systems. Three reference systems are used to describe Micron operations (Fig. 4.5):

- World coordinate (ASAP coordinates)

  This is the reference frame given by the ASAP.

  Once the ASAP is set, this frame is fixed; this is the reason why it is called “world”. This frame is indicated with a “w”;

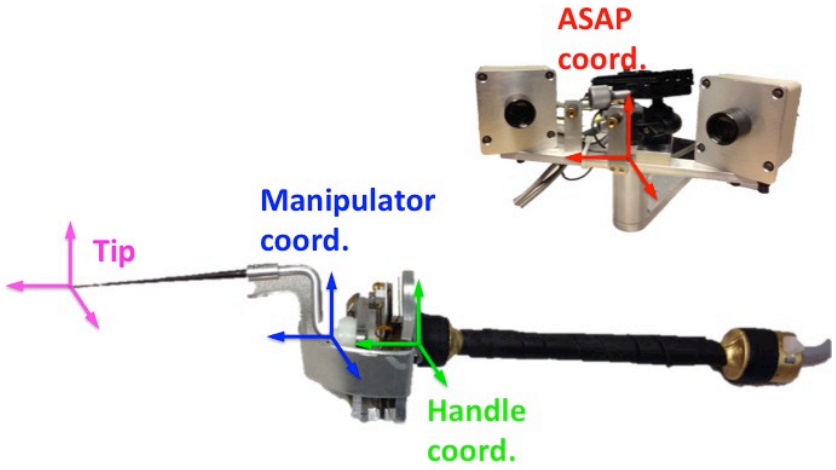

Fig. 4.5: Micron coordinate systems.

- Handle coordinate

  This frame is fixed to Micron handle, so the user moves it in the 3D real space, thus there is a 6-DOF relationship between this frame and the World frame. This frame is indicated by an “h”;

- Manipulator coordinate

  This frame is fixed to the mobile part of Micron (spider and tip), moved by the three stacks. There is a 3-DOF relationship between this frame and the Handle frame because the three motors give 3-DOF. This frame is indicated by an “m”;

- Tip coordinate

  The tip position is determined just by offsetting the manipulator coordinates, since the tip is a rigid tool, thus after a precise tip calibration, the 3D offset between the manipulator frame and the end of the tip is well known.

4.3.2 Micron and human feedback loop

To understand the principles of how Micron system works, a good starting point is Fig. 4.6 that describes a control loop considering a human operator holding a robotic handheld instrument.

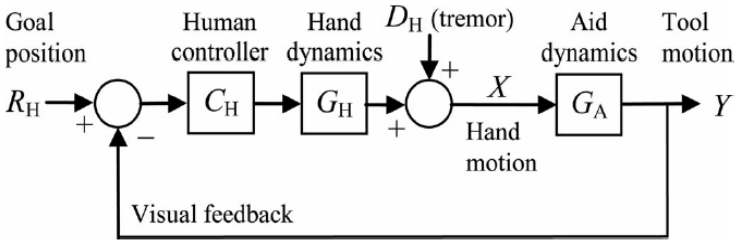

Fig. 4.6: Feedback loop considering an operator holding a handheld active instrument [15]. The handheld active instrument is represented by the G_A Aid dynamics block.

The goal position R_H is the aiming point of the user that is disturbed by tremor D_H, modeled as disturbance. In reality it is something intrinsic of the hand motion. The human controller C_H and the hand dynamics G_H are two blocks to model how the operator tries to control the position and the hand dynamic motion. So the hand motion X is the result of the goal position influenced by the human control and hand dynamics, plus the tremor that degrades the positioning performance.

G_A is the aid dynamics: the robotic handheld manipulator (Micron in this case) that should correct the hand motion, cancelling the tremor. The total hand motion plus the contribution of the aid dynamics gives the final tool motion Y; that is fed back to the operator trough the vision sense (eyes). The human controller C_H, the hand dynamics G_H and the visual feedback are natural motions done by the user.

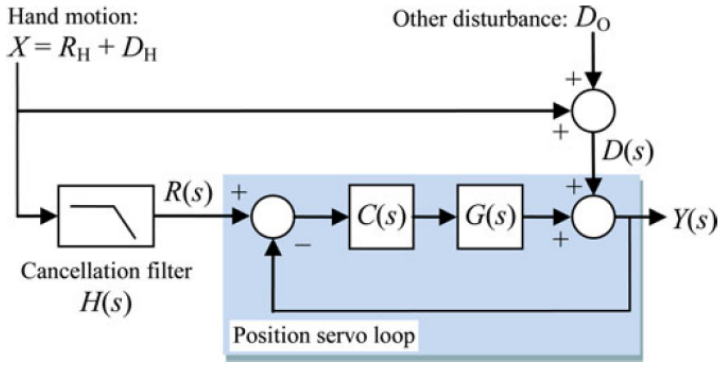

Fig. 4.7: Control loop showing in particular the action of the aid dynamics G_A (handheld active instrument: Micron) [15].

The main interest here is the aid dynamics G_A, where Micron is involved. Fig. 4.7 takes in consideration just the part of interest of the previous control loop, adding more details on how the aid dynamics G_A works.

Also other disturbances are possible during normal surgical operation, for instance coming from the surrounding environment: these are modeled by D_O.

Before entering the position servo loop (light blue rectangle in Fig. 4.7), a c*ancellation (or goal) filter H(s)* is applied. This filter aims to filter out the tremor disturbance and pass only the voluntary motion: *R(s)* is the reference for the position servo loop, that ideally (if *H(s)* filters out perfectly the tremor D_H) is equal to R_H.

G(s) represents the device dynamic effects, and *C(s)* is the controller that has the purpose of compensating for the manipulator dynamics effect.

Thus, if *H(s)* filters out impeccably tremor and the position servo loop (Fig. 4.7) perfectly tracks *R(s)*, then *Y(s)* equals R_H, that is the desired hand position.

The control diagram in Fig. 4.7 represents a single input single output model. But during real operation quantities are measured and expressed in 3D, so a single variable is not enough. The MIMO (multiple input multiple output) system is described in section 4.3.5

4.3.3 Goal position filter

The *goal position filter* (also referred as *goal filter* or *cancellation filter*) *H(s),* is the filter responsible of filtering out the unwanted hand motion, that means the tremor.

As can be seen in Fig. 4.8, Micron has two different filters available: a simple low-pass filter and a scaling-mode (Shelving) filter. Both can be used during Micron operation, using the pedal to switch between them.

Since the motion of the handle and tip in Micron is decupled because there are stacks in between, Micron can implement motion scaling: this is done by a Shelving filter.

Changing the filter corner frequencies f_L and f_H it is possible to “decide” which frequency range motion passes and which is stopped, thus it is possible to modify the signal that passes as wanted motion.

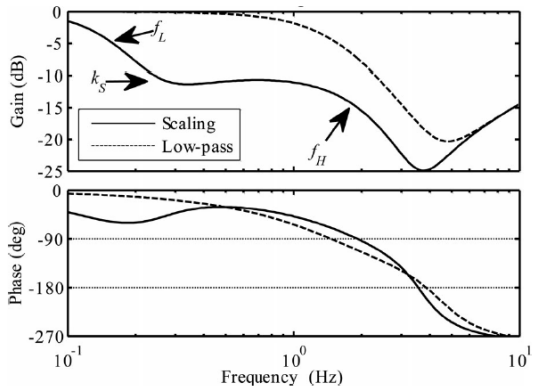

Fig. 4.8: H(s) goal position filter: scaling and low-pass filters [15]. f_L and f_H are the corner frequencies of the scaling filter and k_s is the amplitude of the scaling filter.

These filters were already optimized and the parameters were not changed during this thesis work; these are shown in the following Table 4.1:

Filter	f_L (Hz)	f_H (Hz)	k_s
Scaling	0,15	2	1/3
Low-pass	-	1,5	1

Table 4.1: Cancellation filter parameters [15].

The user can choose between two filters, and according to the behavior of Micron and the task to perform, choose the one that works better. Since this thesis was mainly focused on two tasks of stapedotomy, only the scaling-mode filter was used. This because from previous studies it was observed that better results could be achieved with this filter [15].

4.3.4 Micron controller

The position servo loop in Fig. 4.7 represents Micron controller. More specifically the controller was designed with internal model control (IMC) architecture (Fig. 4.9). IMC was chosen because a frequency domain approach was preferred and it is robust in presence of varying dynamics (tool change).

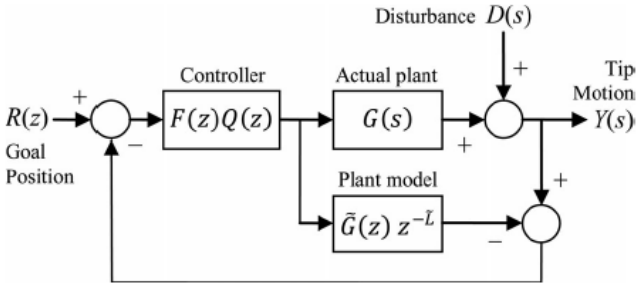

Fig. 4.9: Micron IMC architecture controller.

The actual plant *G(s)* corresponds to the system dynamics that is Micron. The plant model $\tilde{G}(z)z^{-\tilde{L}}$ was determined with system identification (chapter 5.5.2), where $\tilde{G}(z)$ is the model of the system dynamics excluding the controller and $z^{-\tilde{L}}$ models the pure delay of the system, that is the lag of the response given by the control loop and dynamics. If $Q = \tilde{G}^{-1}$, the previous control loop can be simplified as shown in Fig. 4.10.

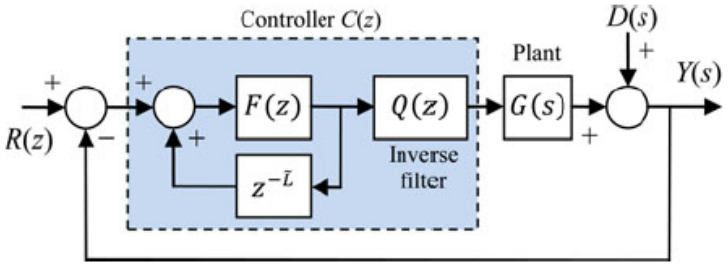

Fig. 4.10: IMC modified architecture, possible when $Q = \tilde{G}^{-1}$.

F(z) and *Q(z)* are functions that are designed to achieve robustness and stable response. *F(z)* is a unity-gain first-order low pass filter with the function of lowering the high frequency modeling error. *Q(z)* instead is called *inverse filter*, in fact if $Q(z) = G(z)^{-1}$, then the output *Y(s)* would eventually be equal to *R(z)*.

Two main parameters of IMC influence Micron dynamics: these are the *F(z)* bandwidth (F_{BW}) and the $z^{-\tilde{L}}$, that is the delay. The user can vary these two parameters from the Micron UI. To see the effect of these changes and

understand which were the values giving the best performance, a step disturbance was injected and the response studied (Fig. 4.11).

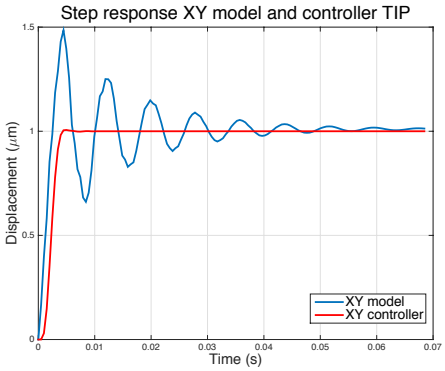

Fig. 4.11: Response of the tip lateral motion to a step of the handle. The step was injected numerically from Micron UI. Plots of system model behavior (blue) and adding the controller (red). The model and the controller were the result of system identification process.

The parameters took in consideration in the response were the overshoot and the rise time.

The effect of the bandwidth and delay is the following:

$$\text{if } F_{BW} \uparrow \Rightarrow \text{Overshoot} \uparrow, \text{Rise time} \downarrow$$

$$\text{if } \tilde{L} \uparrow \Rightarrow \text{Overshoot} \downarrow, \text{Rise time} \uparrow$$

and vice versa.

The best configuration is the one that gives the fastest response, so small rise time, with the smallest overshoot.

It is important to keep the rise time as low as possible so than the human feedback is preserved, otherwise the tip motion can become unintuitive for the user. The overshoot should be low as well to avoid fastidious vibration of the tip that can lead to patient injury.

The parameters were set to: F_{BW}= 150 Hz and $\tilde{L}$= 7 samples.

4.3.5 Micron control loop

The best overview of Micron control system is given in Fig. 4.12, where the MIMO control diagram is reported, considering also the kinematics of the manipulator.

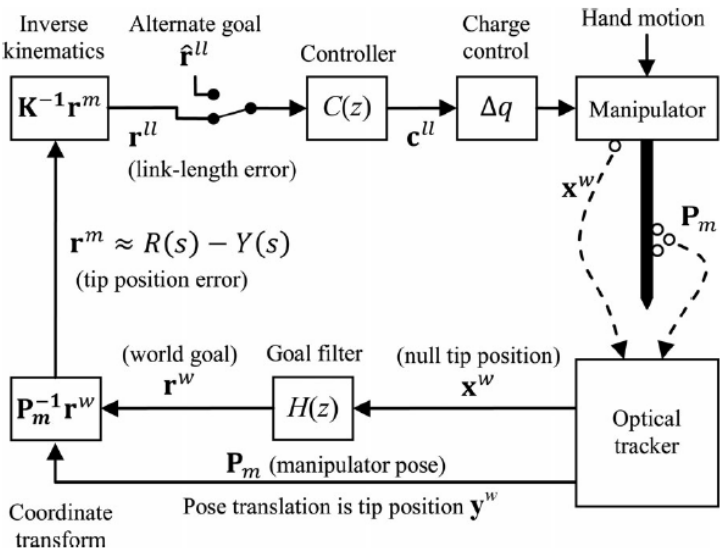

Fig. 4.12: Micron control loop considering kinematics and position vectors [15].

In this chapter the superscript indicates the reference system in which the variable is expressed.

Beginning from the top-right, there is the hand motion of the operator as input. Consequently, the manipulator is moved and this motion is captured by the optical tracking system. Two quantities are measured: the tip and handle position.

Then, x^W and P_m are computed: x^W is the *null tip position*, the position of the tip if the cancellation were off, so with switched off motors. This is the tip position of a non-actuated tool. With cancellation off, the tip position is the same as the handle position.

P_m is a 4x4 linear homogeneous transform that represents the manipulator pose respect the ASAP (world) coordinate.

It should be kept in mind that the manipulator position and the tip position differ only by a fixed 3D offset, so if the manipulator position is known, also the tip position is.

The null tip position (handle position) is than filtered by the *cancellation filter H* to cancel out the tremor and obtain the goal position r^W. Through the matrix P_m the tip position error is computed:

$$r^m = P_m^{-1} \cdot r^W \tag{4.1}$$

This gives an offset, respect to the current tip position that can be seen as an error: the difference between the goal position and the actual tip position.

The matrix *K* represents the *inverse kinematics*, used to transform the error from manipulator coordinate r^m in link-length coordinate r^{ll}: this is the link-length error, how much every link (actuator) needs to move to compensate the position error.

If it is not possible to compensate the error because it is too big that exceeds the workspace, to avoid the motors saturation (and thus the failure of cancellation) an *alternative goal* $\hat{r}^{ll}$ is substituted to r^{ll}. The alternative goal is a position that the tip can reach in the direction of the goal, but with a displacement that is feasible for the motors taking into consideration the limited range of motion.

Then the *controller C(z)* that compensates Micron dynamics, converts the link length r^{ll} into c^{ll}, new link length position. This new link length is then transformed through a charge control to the necessary charge for the motors to reach the new position, since the piezoelectric stacks are charge (and not voltage) controlled. This concludes the operation that Micron control loop makes every cycle. This control loop runs at 2 kHz.

The aim of all previous chapters is to give useful notions to understand the next ones and provide a general background where my research was intended. The main contribution of this thesis was to adapt Micron to the stapedotomy procedure and assess it in real surgical conditions. All that was developed and done is described thoroughly in the following pages.

5 Materials and methods

This chapter describes what was developed and changed to adapt Micron to stapedotomy.

Previous work in this way was done in [33].

First of all, there was the need of an ear model, to understand real dimensions, test instruments and have a deep understanding of surgical conditions.

The tool prototyping and manufacturing required some design and process in beforehand to examine the possible different solutions and analyze them: it required the collaboration of the users (surgeons) and mechanical analysis to understand if the proposed design met the requirements.

After the tools were done, Micron controller needed to be set and configured for the new ones to obtain an optimal tremor cancellation.

All these phases have been the main purpose of this thesis work and are presented and described in the following sections.

5.1 Ear model

At the beginning an artificial ear phantom was developed to test and assess dimensions and provide a working environment.

Surgeons use a funnel shape metal part, called *speculum* that is placed inside the ear canal in order to access the ear. The speculum is a stable surface against which surgeons can rest instruments to reduce tremor and reduce fatigue during the procedure. The speculum, at the beginning of the procedure, is moved freely inside the ear canal, but after the tympanic membrane is lifted up, it is fixed, through a speculum holder, to have a solid resting surface.

The ear model was built accordingly to the one proposed in Fig. 5.1 [13]. In [13], the ear dimensions were deduced from twelve patients' computed tomography scans, taking the biggest dimensions among all the patients, thus maximizing the internal dimension workspace requirement.

The internal workspace is modeled as a cylinder, where the ossicles are situated. The upper part consists of the speculum.

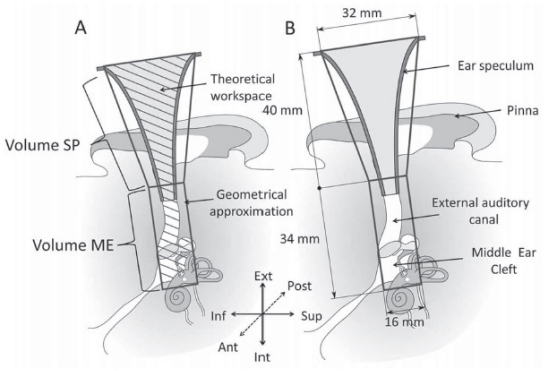

Fig. 5.1: Ear model: dimensions of the ear internal workspace, with maximized dimensions [13]. The internal workspace was approximated to a truncated cone and a cylinder.

Thus the model incorporated an ear speculum, a plastic tube that resembles the ear canal, and a slip of thick paper on which where a stapes footplate-like shape printed (Fig. 5.2).

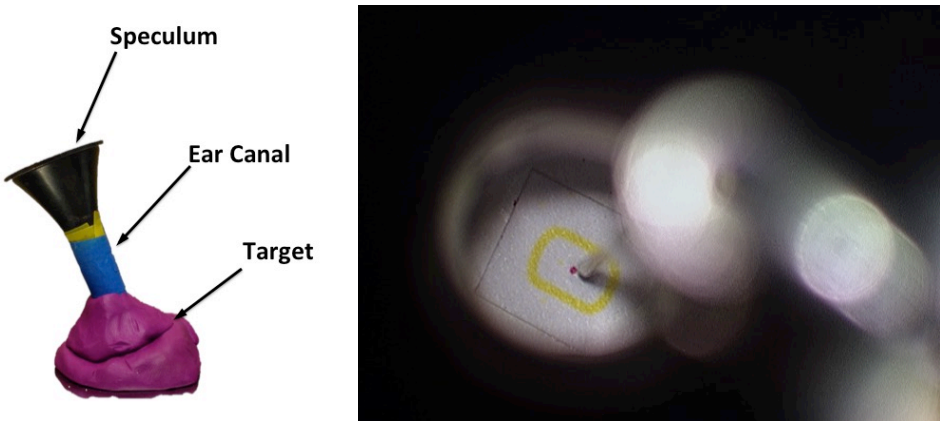

Fig. 5.2: Ear model made with speculum, plastic tube to simulate the ear canal, and a target on the bottom inside the clay layer (left); and the view from the microscope, where the target can be seen (right).

5.2 Tools design and manufacturing

This section goes through the process of design and manufacturing for both tools: fenestrating pick and laser probe.

The tool is the final end mounted on Micron: the actuators move it so that it results stable without the tremor component. The tool tip is the only part that the user can see under the microscope.

5.2.1 Requirements

The tool design had to take in consideration some important requirements that were determined according to: (i) the way the stapedotomy procedure is done, (ii) the surgeon ergonomic and functional desires and (iii) mechanical aspects. These requirements were:

a. Overall length

   The tool has to be long enough to reach the target, that is the stapes footplate, and the surrounding middle ear structures. These dimensions were indicated in the ear model chapter 5.1;

b. No view obstruction

   The tool shape is fundamental to avoid view obstruction as much as possible. Tool, Micron base and hand should not interfere with the sight line;

c. Lightweight

   The tool has to be as light as possible, with the least possible inertia in order to avoid surgeon fatigue. It is an advantage for Micron too, so the tool can be moved more rapidly and reactively;

d. Stiff

   The tool has to be stiff enough to perform the target tasks of stapedotomy without deformation (this also depends on the material);

e. Quickly and easily changeable

   The tool has to be made in a way that the tip can be easily and quickly changed;

f. The tip can be rotated to achieve different orientations

   The tip should rotate of any angle, so the final hook normally present in the ENT surgical tool (Fig. 5.3) can be oriented in different poses according to the surgeon's preference and task to perform;

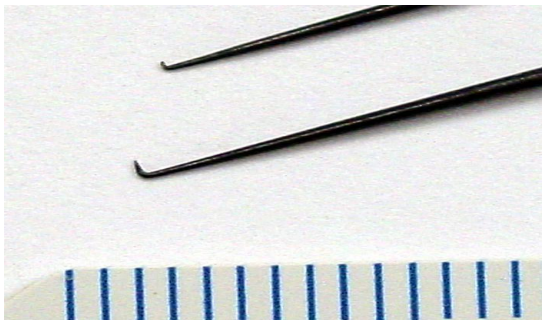

Fig. 5.3: Middle ear surgical instruments hook on the tip.

g. Space for the brace

   The tool shape has to provide space for the brace placement. This because Micron tool cannot be rested against the speculum, otherwise saturation occurs: Micron motors would be constrained vanishing the tremor cancellation effect;

h. Stable tip

   If resonance of the tool happens, the tip would be instable causing unwanted and potentially dangerous vibrations. A positioning error of 1% of the fenestra diameter (800 μm) is considered satisfactory [13], so 8 μm. Thus considered the ASAP accuracy of 4 μm, the tip should not vibrate more than 4 μm at the very end.

These requests were the starting point of the tools design.

5.2.2 Design and manufacturing process

For the tools design, the solid modeling software INVENTOR was used. Through this software parametric 3D models and 2D drawings can be obtained.

The design was made taking into consideration the requirements of the surgeon. Since the beginning, two possible shapes were studied and analyzed. These shapes were inspired looking at some surgical instruments:

- One-bend-shaped tool (Fig. 5.4)
- Two-bends or bayonet-shaped tool (Fig. 5.5)

Fig. 5.4: Bend-shaped surgical tool for ear surgery.

Fig. 5.5: Bayonet-shaped surgical tool used in stapedotomy.

The process of selection had been iterative since several mockups with different shapes and angles were created for testing and assessing the pros and cons. The mockups were used in some ergonomic trials with the surgeon to decide which one was the best shape to use. Comfort, usability and view obstruction were assessed to decide the final tool design.

The tips to be tested were done using a set of telescopic tubes and a needle tip at the end. The part to be attached to Micron was a metal stiff wire bayonet for some configurations and a metal stiff bended wire for the others (Fig. 5.6, Fig. 5.7).

Fig. 5.6: Mockup of the one-bend-shaped tool.

Fig. 5.7: Mockup of the bayonet-shape tool.

The connection between the first part and the tip was done with a piece of heat shrinkable tube.

Many mockups were done with different bayonet height (10–20 mm), bend angles (5-20° for the bayonet-shaped and 20-60° for the one-bend tool) and overall length (tip up to 74 mm).

Surgeons opted for the bayonet-shaped tool since it is more similar to the instruments normally used in ear surgical procedures.

Once the shape was established, the design process continued to meet the other requirements and go towards the definitive tool.

Another step was the choice of the material. Hollow stainless steel tube and aluminum rod were considered, but since the hollow tube is not easy to bend without flatten it, the choice was the aluminum rod. It is cheap, quite easily bendable and light.

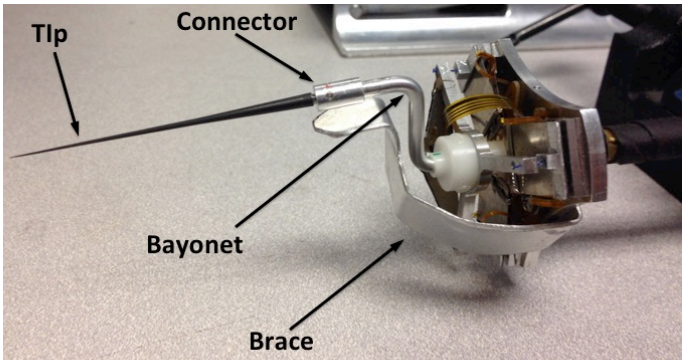

Fig. 5.8: Tool tip (fenestraiting pick) assembly: bayonet-shape, connector and tip.

To complete the requirements of rotation and quick change of the tip, a connector was made (Fig. 5.8). This component connects the S-shaped bayonet

with the tip. It was made of aluminum, to keep the weight as low as possible, with a press fit connection on the bayonet side and a slide connection on the tip side, so the tip can be easily and rapidly changed. This connection was designed cylindrical, so the tip could rotate to achieve different orientations. To block the tip in a desired position, two setscrews were placed in the connector: screwing those two setscrews the tip could be blocked. Unscrewing the setscrews the tip is free to slide and rotate, so it can change orientation or be removed.

The tip was not directly manufactured, since it was really thin and the material had to have high mechanical characteristics. The decision was to take a surgical instrument used for ear surgery, cut the tip about the right length and mount it into the connector. The tip was manufactured at the workshop of the university (Carnegie Mellon University), since the bottom of the tip needed to be cylindrical to fit inside the connector hole. Particular attention was paid to tolerances: the connection had to be a slide fit.

During stapedotomy laser is used as well. It is needed to perform a rosette onto the stapes footplate.

Since the objective is to evaluate Micron during a real procedure (chapter 2.3.1), a laser tool was designed and made (Fig. 5.9). The first parts (bayonet mount and connector) were in common with the previous tool, but the final tip changed. The tip had to house the optical laser fiber: this was an OmniGuide BeamPath OTO-S CO_2 laser fiber, protected with an outer jacket and with a final metal end, important to keep for preserving the optical characteristics of the laser spot.

The laser tool was made by hollow hypodermic tube glued together with the metal final end of the CO_2 laser fiber.

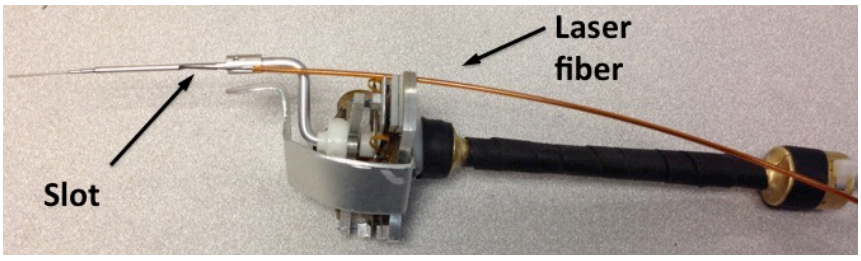

Fig. 5.9: Laser tool for Micron.

The laser fiber came from the side of the tool, so a slot was done in order to pass the fiber inside the hollow tube and glue the final metal fiber end on the tube. In this way the metal head of the CO_2 laser fiber was preserved, thus not altering the optical characteristics of the laser spot.

5.2.3 Workspace analysis

To understand the differences between different tool shapes and have a practical indication of the range of motion of the end effector, workspace analysis was done.

To compute and plot the workspace MATLAB was used. The actual bayonet-shape tool was implemented.

According to [34] the workspace representation for parallel robots is only possible if the robot is 3-DOF. Micron has 3-DOF and so the workspace can be computed and plotted.

There are different types of workspace that can be computed for a parallel robot: the type aimed depends on what information is needed. The information needed in the current case was the maximum possible workspace, so all the positions that the tip can reach, whatever orientation of the platform or position of the links (obviously keeping the handle fixed in one position). This is meant to be the *maximal workspace* or *reachable workspace*.

The first assumption is that Micron geometry is perfectly known, but measuring or manufacturing, errors may always be done.

Since Micron is 3-DOF, 3 independent variables were chosen. Those were:

- The angle of rotation along the x-axis (ϑ_x) ;
- The angle of rotation along the y-axis (ϑ_y);
- The displacement along the line from the center of the moving plate (tool insertion point) to the tip of the tool (Δl).

The initial position (Fig. 5.10) is when the base and the moving plate (refereed from now on as plate) are parallel and centered. The center O of the reference system is taken at the center of the plate.

The base vertexes are fixed and labeled as B_i. These points are the bottom of each of the three stacks. The F_i points represent the end of each stack and the beginning of the flexures that connect the stacks to the base plate. In the model

the F_i points are constrained to move only along the Z-direction, constraint imposed by the stack geometry. Finally the P_i points describe the vertexes of the moving plate. The center of those points is the center of the reference system. This reference system was the same used during Micron calculation and operations in real time.

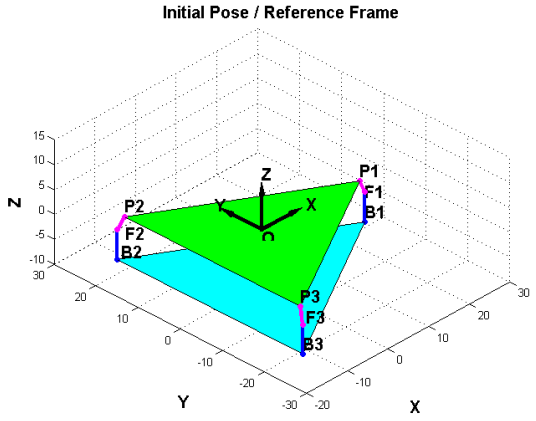

Fig. 5.10: Initial configuration and reference frame of Micron. The P_i points are the vertexes of the moving plate; the F_i are the points that connect the flexures and the stacks and B_i are the base points. The green patch is the moving plate; instead the cyan one is the fix base.

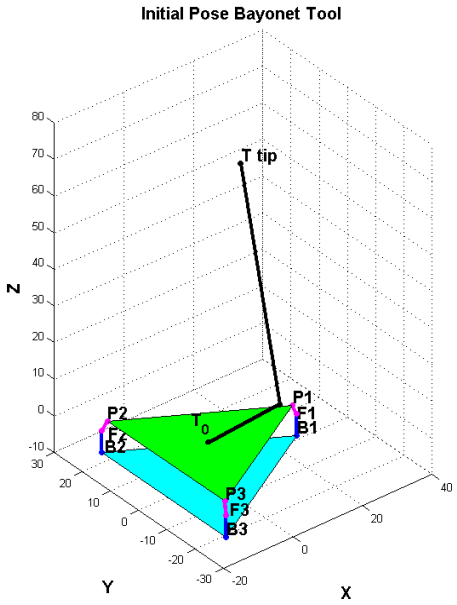

Fig. 5.11: Initial pose: bayonet-shaped tool configuration. The bayonet is modeled as two segments, but the important point is the tool tip (T tip).

Important to notice that the flexures undergo a complex non-linear deformation, but here they are modeled as rigid links with fixed length. No constraint is imposed on the angles between the flexures and the plate or the links, so they can move in the 3D space with no restriction: this is not an unreal approximation since the angular range of motion is less than 2°. The movement is imposed by the plate, moving according to the three variables ϑ_x, ϑ_y, Δl.

The code was implemented to make the calculation described below. The bayonet-shaped tool was modeled as two segments, as shown in Fig. 5.11.

The initial pose was known, so the coordinates of each point were notorious:

$$B_i = \begin{bmatrix} b_{i,x} \\ b_{i,y} \\ b_{i,z} \\ 1 \end{bmatrix}, \quad F_i = \begin{bmatrix} f_{i,x} \\ f_{i,y} \\ f_{i,z} \\ 1 \end{bmatrix}, \quad P_i = \begin{bmatrix} p_{i,x} \\ p_{i,y} \\ p_{i,z} \\ 1 \end{bmatrix}, \quad T_{tip} = \begin{bmatrix} t_x \\ t_y \\ t_z \\ 1 \end{bmatrix} \tag{5.1}$$

being the index i from 1 to 3.

To draw the workspace a range was assigned to the three independent variables ϑ_x, ϑ_y and Δl. This range exceeded the real configuration, but at the end all the results not compatible with the motors rage of motion (±400 μm) were rejected.

The unit vector that represents the tool is known, since the starting and final points of the tool are known; this vector is called $\boldsymbol{n_{tool}}$.

For every ϑ_x and ϑ_y angles the respective rotation matrix R_x and R_y (3x3) were calculated:

$$R_x = \begin{bmatrix} 1 & 0 & 0 \\ 0 & \cos(\vartheta_x) & -\sin(\vartheta_x) \\ 0 & \sin(\vartheta_x) & \cos(\vartheta_x) \end{bmatrix} \tag{5.2}$$

$$R_y = \begin{bmatrix} \cos(\vartheta_y) & 0 & \sin(\vartheta_y) \\ 0 & 1 & 0 \\ -\sin(\vartheta_y) & 0 & \cos(\vartheta_y) \end{bmatrix} \tag{5.3}$$

Then the $\boldsymbol{n_{tool}}$ vector is rotated in the new direction to obtain $\boldsymbol{n_{new}}$:

$$\mathbf{n}_{new} = R_x \cdot R_y \cdot \mathbf{n}_{tool} \tag{5.4}$$

At this point the orientation of the new pose is known, and since the plate has moved, also the starting point of the tool (center of the plate) is changed:

$$O_{new} = \Delta l \cdot \mathbf{n}_{new} \tag{5.5}$$

Now the roto-translational matrix (4x4) can be determined:

$$R = \begin{bmatrix} R_x \cdot R_y & O_{new} \\ 0 \quad 0 \quad 0 & 1 \end{bmatrix} \tag{5.6}$$

To determine the new position of the P_i points a multiplication is made:

$$P_{i,new} = R \cdot P_i \tag{5.7}$$

At this point the only unknown was the z-coordinates of the F_i points, because those points are constrained to move only along the z-direction. Also the distance of the flexures (*PF*) remains constant during the manipulator motion:

$$PF = \sqrt{(p_{i,x,new} - f_{i,x})^2 + (p_{i,y,new} - f_{i,y})^2 + (p_{i,z,new} - f_{i,z})^2} \tag{5.8}$$

Thus the z-coordinate of the flexure points can be computed:

$$f_{i,z} = p_{i,z,new} - \sqrt{PF^2 - \left[(p_{i,x,new} - f_{i,x})^2 + (p_{i,y,new} - f_{i,y})^2\right]} \tag{5.9}$$

So now all the new points coordinate are determined, and the length of each link (*ll)* can be calculated:

$$ll_i = \left|\left|P_i - F_i\right|\right| \tag{5.10}$$

At this point for every configuration (ϑ_x, ϑ_y, *Δl)* the length of the actuator *ll* was checked. The stack motion is ±400 μm nominal. So:

If $ll_i > 400$ μm → invalid position

If $ll_i < 400$ μm → valid position

At the end, all the valid positions form the workspace of Micron, shown in Fig. 5.12.

The workspace has approximately the shape of a squashed cube; the volume is circa 3,5 mm^3, calculated measuring three sides of the cube.

The usual dome-shape obtained for the 3-DOF parallel robots here cannot be seen, because of the limited range of motion of the stacks. Indeed according to [15] the angular deflection of the tip is less than 2°.

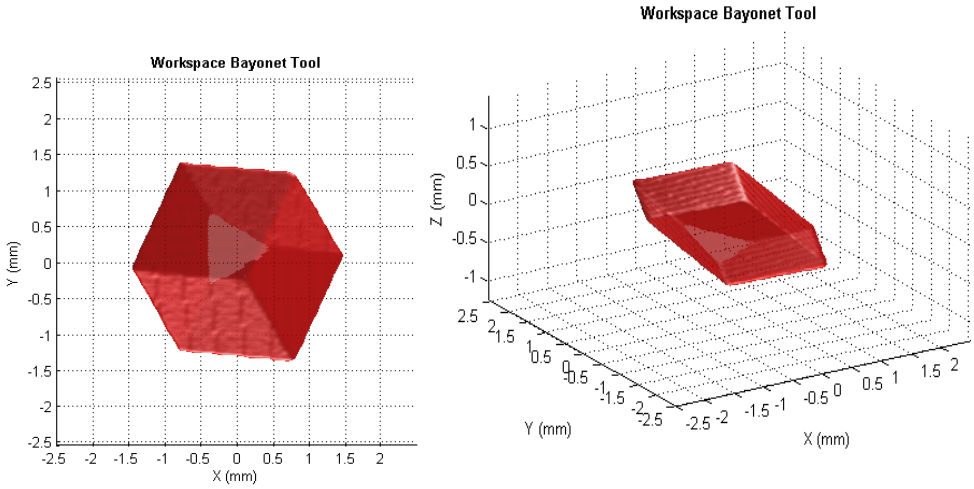

Fig. 5.12: Bayonet-shaped tool configuration workspace. The shape of the workspace is a squashed cube that can be seen in the xy-plane (left) and in 3D space (right).

5.3 Brace design

The brace was designed for several purposes that are listed below:

- It provides protection of the tool. The tool has to be free to move since the motors are moving it. If it is in contact with a surface or blocked, saturation occurs: the motors cannot move the tool anymore and then the tremor cancelling effect is lost;
- The brace can be rested against the speculum. In this way the tool is free to move and the surgeon can rest the hand against something fixed and solid. This allows achieving better movement precision and reduces the hand tremor and fatigue.

The brace has a fairly complex shape because it is bent along several planes and it needs to be well-centered respect to the tool. It is fixed to Micron base through a screw and a nut. Unscrewing the nut, the brace can be easily removed.

The final brace can be seen in Fig. 5.8 and Fig. 5.9.

5.4 Handle design

The initial handle of Micron was a cylindrical plastic shaft, with a smooth surface as can be seen in Fig. 5.13. The handle houses the cables coming from the electronics, which pass inside and connect with the actuators.

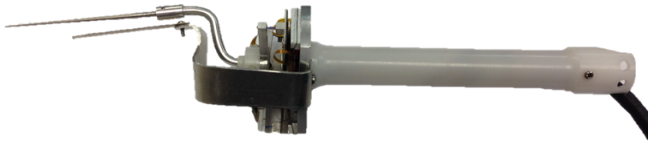

Fig. 5.13: Micron with the old plastic white handle. The tip and brace where initial prototypes.

There was a redesign of the handle by two previous students working on Micron. That handle was more ergonomic: the shaft was smaller in diameter so the hold was more natural, there was a knurling to enhance the grip. At the bottom, there was an enlargement to house cables. The handle was made by two parts, o it was easier to mount and take off without having troubles with cables.

Fig. 5.14: Previous plastic handle.

This handle was too short, thus disturbing during the hold. The cylindrical enlargement at the bottom created disturbance. Also the knurling features were too high, uncomfortable at the touch. So a new design was proposed and manufactured, as can be seen in Fig. 5.15.

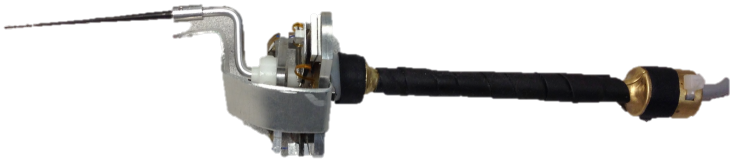

Fig. 5.15: Micron handpiece with the new re-designed handle.

The important changes done were:

- Firstly the new handle was longer, so the enlargement at the bottom is not disturbing during the holding;
- Secondly, the material is changed: a metal material was preferred. The best one happened to be brass. It combined the fact that thin wall thickness can be achieved through the process of 3D printing (minimum wall thickness 0.5 mm), and the cost is not high;
- Thirdly, the bottom part is changed becoming bigger, having more room for the cables;
- Fourthly, it was taken the decision to replace the knurling with some grip tape. The design became easier: the problem of the feasibility of small details and feature with the 3D printer technique was avoided.

The 3D printing technique, as said, was chosen to manufacture the handle, since it is pretty cheap and allows great shape freedom.

5.5 Control tuning and calibration

This section goes through the different calibrations necessary to obtain an optimized tremor cancellation with Micron. Then the important part of system identification is described, necessary procedure to compute a dynamic model of Micron and implement it in the control loop.

5.5.1 Calibrations

For an optimal use and to achieve the best tremor cancellation, Micron needs to be calibrated. There are four types of calibrations: ASAP sensor, ASAP light (LEDs), tip offset and inverse kinematics calibration.

The ASAP sensor and light calibrations are done once, since they do not depend on the type of tip that is the only interchangeable piece during Micron operations. On the other hand, the tip offset and inverse kinematics calibration have to be done every time the tool is changed.

- ASAP sensor calibration: this is a one-time calibration, unless mechanical changes are made to the position of the PSD cameras. This procedure aims to calibrate the optical parameters and the analog phase of the cameras. It calibrates the position of the cameras respect to the ASAP coordinate system (world coordinates);

- ASAP light (LEDs) calibration: LEDs require calibration with respect to the manipulator coordinate system. The first step was to determine the position of the lights with respect to each other, then the position of the light-center is calculated respect the manipulator coordinate system;

- Tip offset calibration: the tip offset is the position of the tool tip in manipulator coordinate system. So if a new tip is mounted, the tool tip position changes and a new calibration is needed. The calibration is done by using a pivot procedure: a fixed point is taken and Micron is positioned in different poses by placing the tip at the same fixed pivot point. This is done with the help of a microscope;

- Inverse kinematics calibration: this procedure compensates for floats in the open-loop electro-mechanical behavior of Micron. This is also a good way to check the right functioning of the system. After clamping Micron in a vice, the calibrate kinematics UI is used. This UI moves the tip and computes the inverse kinematics matrix, which is the result of the kinematic calibration procedure.

When all those procedures are done, Micron is ready to be used, with its optimized cancellation parameters.

5.5.2 System identification

System identification is a process that aims to compute a mathematical model of a system without knowing exactly its physical equations and the process going on. A mathematical relation between an input and output is sought: a model that, with the given input, produces the output response is the target. When such a

model is found the last step is the validation process to assess the model performances.

There are two possible approaches for system identification:

- Grey box model

  The model structure is known formerly from physical principles, but the model parameters are still unknown. The process of the system identification in this case aims to determine the parameters so that the model fits the measured data;

- Black box model

  In this case the model structure and its parameters are totally unknown. A correlation between input and output is sought regardless of the model structure. The process is iterative, since many different models are tried, with different orders, and the performance is compared at the end, finally choosing the best one. This approach is used when the best fit of the model to the data is wanted, but there is also a trade-off between data fit and complexity of the model.

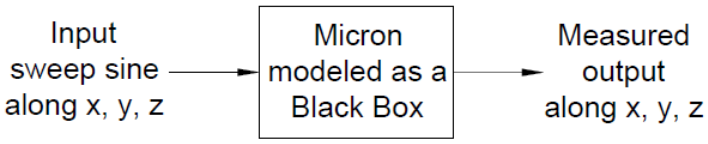

Fig. 5.16: Black box model for system identification.

Micron is a complex system and deduction of the model from physical principles is too laborious, thus black box model was used (Fig. 5.16).

The aim of system identification in this case was to find a linear, discrete-time model of Micron dynamics, excluding the controller. This means to determine $\tilde{G}(z)z^{-\tilde{L}}$, needed in Micron controller (chapter 4.3.4), thus also the inverse filter since $Q = \tilde{G}^{-1}$.

System identification procedure is here described step by step:

1. Sweep signal injection (input signal)

A sweep-sine signal (Fig. 5.17) was used as excitation signal (input) along each of the three axes of the tip: x, y and z.

Since the stimulus (excitation signal) was injected in the stack space, the amplitude of each motor motion, which results in the motion of the tip along one Cartesian direction (x, y or z), is needed.

The amplitude of each motor displacement, for obtaining the wanted tip movement, was given by multiplying the inverse kinematics matrix IK (3 × 3) with the wanted motion of the tip. For instance, the motion amplitude of each stack to obtain a movement of the tip along the x-axis is computed like this:

$$[IK]\cdot\begin{bmatrix} x_{tipMotion} \\ 0 \\ 0 \end{bmatrix}=\begin{bmatrix} A_{Stack1} \\ A_{Stack2} \\ A_{Stack3} \end{bmatrix} \tag{5.11}$$

Being IK the inverse kinematics matrix, $x_{tipMotion}$ the wanted movement along the x-axis and $A_{stack\ i}$ the motion amplitude of each motor to reach the desired tip motion. Same operation was done to obtain the y and z motions.

So every motor was moving like a sweep sine with amplitude given by the result of the previous operation.

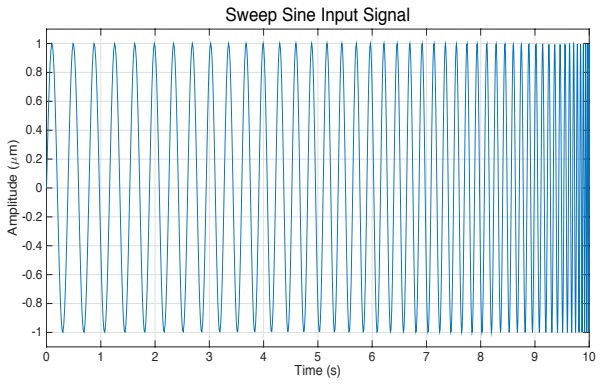

Fig. 5.17: Stimulus: sweep sine input signal. Frequency range: 5-1000 Hz. The length of the input signal was 10 s.

The frequency range of the sweep sine injected (Fig. 5.17) was chosen from 5 to 1000 Hz. This is the frequency range of interest.

The manipulator resonances are unknown before system identification process. However because of the general dependence of resonance frequencies form the square root of mass and compliance, in practice, a structure needs to be quite heavy and/or flexible to have resonances below 10 Hz and Micron is quite stiff and light (≈ 75 g).

2. Data generation and collection

Micron was run injecting the sweep sine signals for each motor as input and the collection of output data was done from the Micron UI. These data are in the stack space (link length of the motors), since the controller and the inverse filter run in stack space (see Fig. 4.12).

This operation was done for both the tools: fenestrating pick and laser probe.

Output data collected were the combination of eight runs, using averaging technique. The averaging technique overlaps many times the same suppose signal, helping to reduce the noise influence on the signal and increasing the signal-to-noise ratio; this is done under the hypothesis that the noise is random and it is uncorrelated with the signal.

3. Data analysis and models generation

Data were processed and analyzed using MATLAB, in particular operating with the system identification toolbox. Spectral frequency responses were computed from the time domain data (Fig. 5.18).

This was done for two different tools: the surgical instrument tip (fenestrating pick) and the laser probe.

It can be noticed that the x and y frequency response are quite similar in both the plots (dotted lines). This happens because Micron has a parallel configuration, and lateral motion is obtained moving opposite motors, instead axial motion is obtain differently, moving all the three motors together.

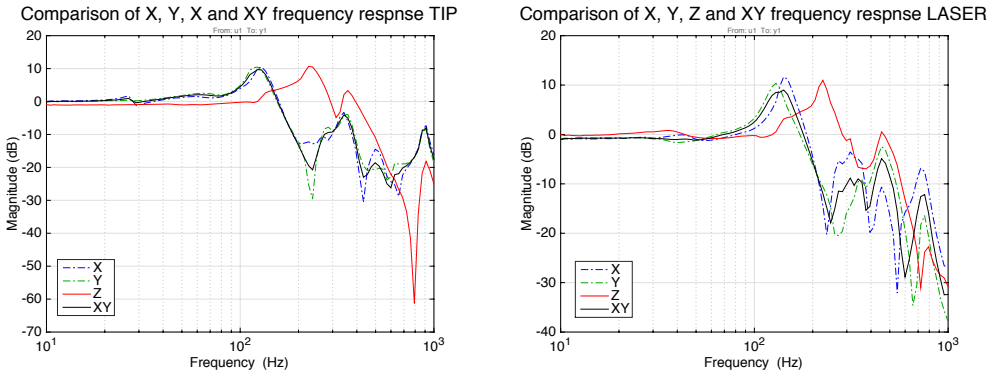

Fig. 5.18: Tip (left) and laser (right) tool frequency response.

Because of this similarity, the *x* and *y* frequency responses are combined, to form an average model *xy*. This average model is obtained by adding the x and *y* time domain data together, one after the other, and computing the frequency model of the $x + y = xy$ frequency response. So at the end the only frequency response considered were the *xy* for the lateral motion and the *z* for the axial.

Once the frequency response was computed, a model was needed for each direction. Using the Matlab toolbox, several models with different orders were tried to fit the frequency response curves (*black box modeling*). At the end the *state space* model was chosen to be the best model structure to fit the spectral data.

Two state space models were generated for *z* and *xy* responses: one with higher order for the best data fit, called "*model*", and another one that had a good fit too, but with lower order, called "*reduced model*".

Initially a model was estimated at the lowest order that reasonably captures the full frequency response: the interesting frequency range was 10 – 500 Hz. The focus was on that range to reduce the model order; this because the first resonance is around 100 Hz.

The model curve should fit the Bode plot of the frequency response, considering both the magnitude and phase. This was done through the *prediction error minimization*, algorithm that determines the parameters of a model of given order to fit a certain data set. The result was a state space model, with the number of states according to the given order.

Then an *order reduction* was performed to drop out states of no interest for modeling. This was done using the MATLAB command *balred* that computes the reduced-order model discarding the small *Hankel singular values*, i.e. the states with low-energy.

Multiple reduced order model were tried to determine the best one. The order reduction helps to obtain a more manageable and understandable model, and a faster computation.

Fig. 5.19 and Fig. 5.20 display the model and reduced model frequency responses. Models *xy* and *z* for the fenestrating pic have an order of 10 (number of states), the reduced models instead are of order 8. For the laser probe the model has 12 and 14 states for *xy* and *z* respectively, the reduction lowers the states to 6 and 8.

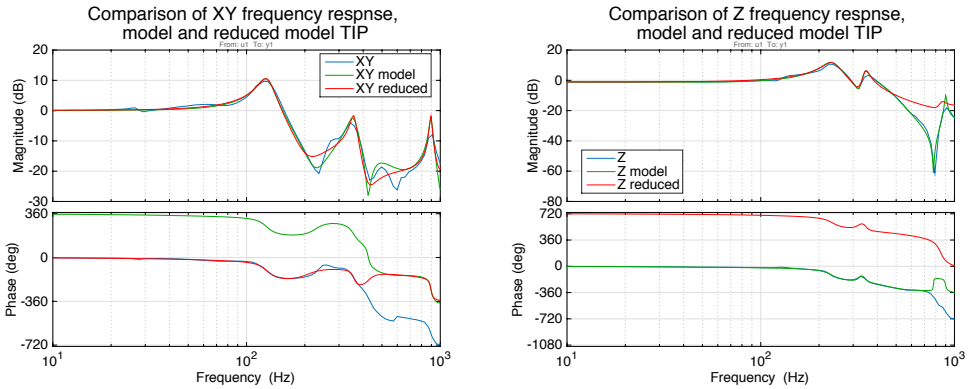

Fig. 5.19: xy (left) and z (right) frequency response, model and reduced model comparison, for the fenestrating pic.

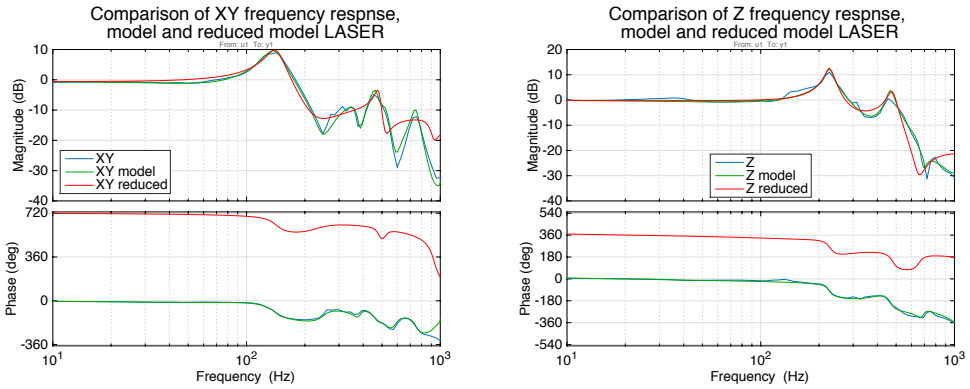

Fig. 5.20: xy (left) and z (right) frequency response, model and reduced model comparison, laser probe.

After this phase, the validation of models was done, checking the fit of the models paying attention to the Bode plot of the magnitude and phase in the frequency range 10 – 500 Hz. The focus on this frequency range allowed reducing the model order, since higher resonance frequencies are less important and cause the model to be more complex because of the higher order, thus introducing more phase lag. The mean and modified xy model was taken as a reference to design the lateral controller. The z-reduced model was taken as reference to design the z controller.

4. Controllers generation

The ideal controller corresponds to the inverse dynamic of the models; but this operation, most of the times, generates an unstable response, due to the presence of unstable poles and zeros. Thus the controller was generated by

- Inverting the *xy* and *z* reduced models;
- Dropping the unstable poles and zeros;
- Adding two conjugate pairs of poles from a low-pass Bessel filter (4^{th} order). The addiction of the Bessel's filter poles gives a low-pass characteristic to the result.

After the inversion, the poles with low damping that can generate instability [35] are "corrected" augmenting their damping to 0.1, so to increase the damping and obtain a more stable response.

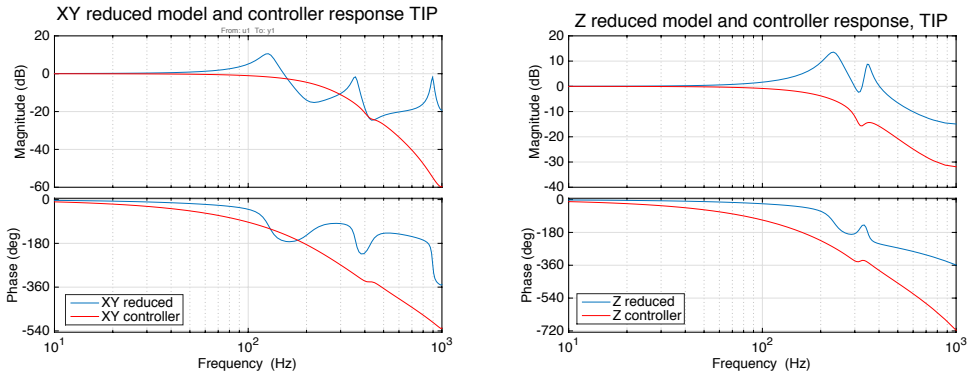

Fig. 5.21: Tip xy (left) and z (right) reduced model and controller frequency response (Bode plot).

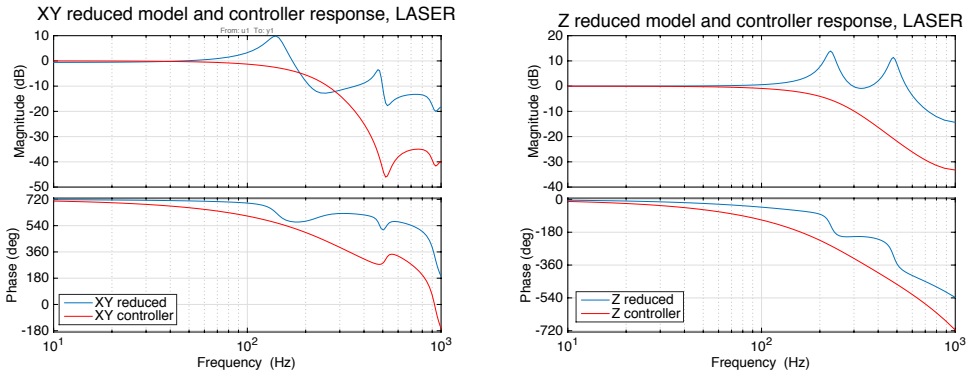

Fig. 5.22: Laser probe xy (left) and z (right) reduced model and controller frequency response (Bode plot).

In Fig. 5.21 and Fig. 5.22 there are plotted the *xy* and *z* "reduced" model (that models Micron without controller) and the *xy* and *z* "controller", that is the system with the controller, obtained by the multiplication of the transfer function of the reduced model and the filter obtained by inverting the model and keeping only the stable zeros and poles, and modifying the unstable one, in the frequency range of interest.

If the model from the system identification differs a lot from the real system, the control system will not work optimally calculating a wrong error and so a wrong motor displacement to correct the position of the tip: the outcome would be a bad tremor cancellation. But this was not the case since the goodness of cancellation was tested before the trials injecting a step stimulus and analyzing the response (overshoot and rise time) and making some practical trials Micron "hands on".

6 Experiments

The general objective of this research is to improve positioning accuracy and precision of the tool in otologic microsurgery using Micron. More precise manipulation will lead to better clinical outcomes and reduce complications.

The specific aim is to compare performance in stapedotomy with and without the assistance of Micron.

To assess the effect of Micron and the developed designs, experiments were performed. The design of experiments is described in the following sections.

6.1 Experiment configurations

The trials were performed using two different configurations of Micron:

- Unaided: Micron off

  The cancellation of tremor was off. So Micron was used as a conventional surgical tool: the motors were inactive and the tip was moving accordingly to the handle.

- Aided: Micron on

  The cancellation was on, so Micron deflected its tip to counteract the human tremor: the motors moved the tip cancelling the unwanted components of the handle motion. This is the case of active tremor cancellation device.

The target used for the model-trials was the ear model developed, that can be seen in Fig. 5.2.

After that, some other trials were performed on cadaver's temporal bones. These bones have the ear canal (the circular hole in the center of the bone in Fig. 6.1)

with the auditory ossicles inside; so getting rid of the tissue and bones, the stapes footplate can be addressed. This operation was done before the trials.

Model-trials and bone-trials steps are described in the following chapter.

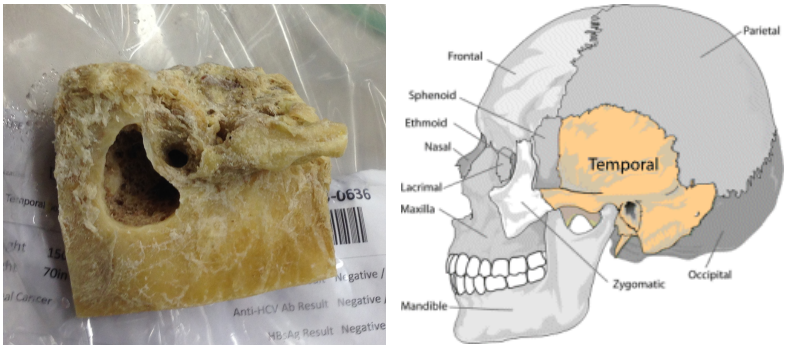

Fig. 6.1: Temporal bone (left), and its location (right) in the human skull [http://wellnessadvocate.com/?dgl=10232, 2014.12.6]. The round hole in the center of the temporal bone is the ear canal.

The order of the test condition was varied to exclude the effect of order biasing the result. For every session one aided and one unaided trial were done. The order is shown in Table 6.1 and Table 6.2:

Model trials	Session 1		Session 2		Session 3		Session 4		Session 5	
Surgeon 1	On	Off	Off	On	On	Off	Off	On	On	Off
Surgeon 2	Off	On	On	Off	Off	On	On	Off	Off	On

Table 6.1: Model trials order: succession of aided (On) and unaided (Off) case.

Bone trials	Session 1		Session 2	
Surgeon 1	On	Off	Off	On
Surgeon 2	Off	On	On	Off

Table 6.2: Bone trials order: succession of aided (On) and unaided (Off) case.

The user holding Micron can feel the difference between Micron on and off: when cancellation is on and motors are working, an electric flow can be sensed through the handle. The human visual feedback recognizes as well that the tip is actuated. Because of this, while Micron is on, the tests cannot be completely blinded.

Two surgeons accomplished trials: the first surgeon (Surgeon 1) was an experienced ENT surgeon, specialized in ear surgery. The second one (Surgeon 2) was younger, a fellow. He was at the end of his fellowship, focusing in ear procedures. So they were both skilled and well-trained surgeons in ear operation, but the experience level was different.

6.2 Experiment steps

In the following section the setup for the trial using the model and the bones is described.

6.2.1 Bone trials

The aim of these experiments was to perform an ideally circular hole (fenestra) on the stapes footplate.

The task was performed using Micron in two different configurations (Micron on/off) and using two tools: a laser tool and a fenestrating pick. The two different tools were mounted on Micron, leaving the bayonet, connector and brace in position and changing only the end part.

The piece of temporal bone was fixed using a temporal bone holder. Above the temporal bone and in contact with it, there was the speculum. This was fixed using a speculum-holder, to avoid its movement. The fixation of the parts was done to simulate the real operation conditions. The speculum and the speculum-holder are instruments used in the OR as well (Fig. 6.2).

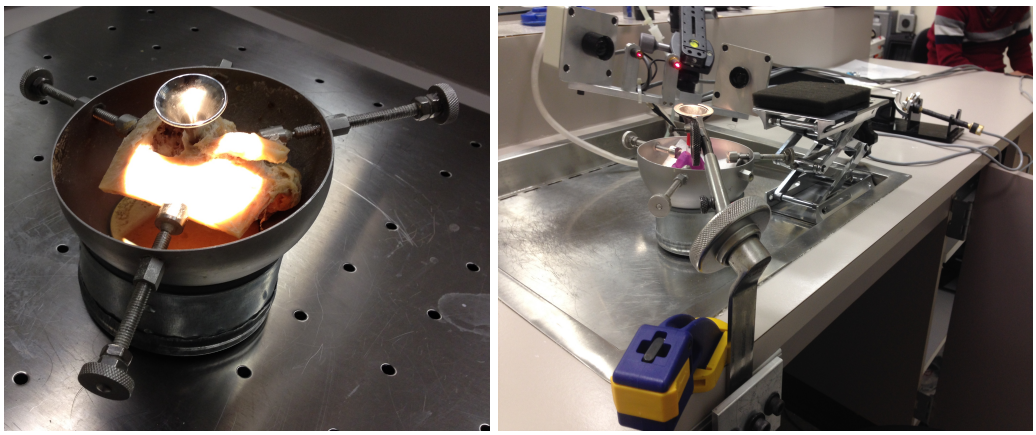

Fig. 6.2: Temporal bone holder (left) and experiment configuration with temporal bone holder, speculum, speculum holder and hand rest (right).

A microscope was used to see the target inside the ear canal. Different magnifications were used, accordingly with surgeon's preference (the mostly used ones where 16x and 25x). Close to the speculum, a hand-rest was placed to simulate the patient's head where the surgeon could rest the forearm or hand.

Fig. 6.3 shows the experiment setup, highlighting all the components.

Fig. 6.3: Experiments setup. All the components can be seen: 1) Micron, 2) target (bone in this case) and bone holder, 3) speculum, 4) speculum holder, 5) ASAP, 6) microscope, 7) laser machine, 8) hand rest.

Surgeons were asked not to touch the speculum with the tip while using Micron, since we would like to evaluate the effect of Micron during the cancellation and therefore the motors should be free to move the tip without constraints. The brace placed on Micron was to avoid saturation of motors. In order to keep the brace as small as possible, and to create as low disturbance as possible, in some position the tip could still touch the side of the speculum.

After the preparation of temporal bones, the trials steps were as follow:

1. Decide the center of the rosette

   Decide where the ideal center was. This was done with a laser burst;

2. Perform the rosette

   Micron with the laser probe was used to perform the rosette. The CO_2 laser was set in pulsating mode with power and impulse time decided beforehand. It is easier to perform the rosette by overlapping each laser burst slightly. The ideal diameter is 0.8 mm and the ideal shape is a circle. Before the next step a photo was taken;

3. Touch the stapes footplate with the fenestrating pick

   The surgeon was asked for three times, using the fenestrating pick, to go down as straight and perpendicular to the footplate as possible until touching its surface. This operation was needed to compute the depth penetration (see chapter 6.3.2);

4. Working with the fenestraiting pick

   The surgeon at this point removed bony material inside the fenestra, so than a hole in the stapes footplate was opened. A last photo was successively taken. This was the end on the trial;

5. Measurements

   At this point the trial was ended and all the important variables were measured to assess the shape and the quality of the fenestration and make a comparison between different configurations: the measurements were done afterwards using image processing techniques and data analysis, using photos, videos and data collected during each trial.

6.2.2 Model trials

Model trials were done before the bone ones. This was done for the surgeon to acquire more experience handling Micron before the bones, that is a much more difficult condition compared to the model.

For the model trials the process was shorter, with less steps. The fenestrating pick was not used since the only task in these sessions was to perform the rosette.

The trials in this case were limited to the rosette task, thus only the laser tool was needed.

The model sessions were more than the bone ones; this was due to the limited availability of bones. These bones were form cadavers, and they are pretty costly.

6.3 Measured variables

To compare performances between aided (Micron on) and unaided (Micron off), the following variables were measured or computed:

- Fenestra size and geometry

  The fenestra size is ideally circular, 0.8 mm in diameter. Image processing techniques (chapter 6.3.1) were used;

- Completion time

  Time needed to complete the fenestration was recorded;

- Penetration depth

  Depth penetration is crucial in this step of stapedotmoy: if the instrument goes too deep there is the risk of inner ear structures damage. Data from Micron optical tracker were used to measure and compute penetration depth. The surgeon was asked to touch several times in different points the surface of the stapes footplate: those points were used to assess how deep the user had

gone during the trial. This measure was done only in the bone trials. For the method description see chapter 6.3.2

In bone trials data were recorded while the rosette was performed and after that, when the fenestrating pick was mounted to understand how deep the tool went compared to the zero-plain defined by touching the stapes footplate.

6.3.1 Image Processing and Measures

Model trials

To quantify the goodness of the rosette some parameters were recorded and computed. To analyze the shape of the rosettes, a GUI (graphical user interface) was developed (Fig. 6.4). The image was:

a) Turned from colored to black and white and a Gaussian filter was applied to eliminate noise;
b) A thresholding technique was applied to identify only the rosette shape;
c) The contour was detected;
d) Centroid, best fit ellipse and equivalent circle were plotted;
e) Knowing the pixel to μm ratio of the pictures taken with cameras through the microscope, numerical results were computed.

This was done for the rosettes of every trial.

The following parameters were computed and investigated through the image processing GUI (Fig. 6.4):

- Eccentricity (*e*)

  This number indicates how much a shape deviates form being circular. The lower the eccentricity the more circular is the shape. The eccentricity of a circle is zero; the eccentricity of an ellipse is greater than zero but less than one. If the eccentricity is one, then the shape is a line. The eccentricity *e* is computed as follows:

$$e = \sqrt{1 - \frac{b^2}{a^2}} \tag{5.12}$$

being *a* and *b* the length of the semi- major and minor axis of the best fit ellipse respectively;

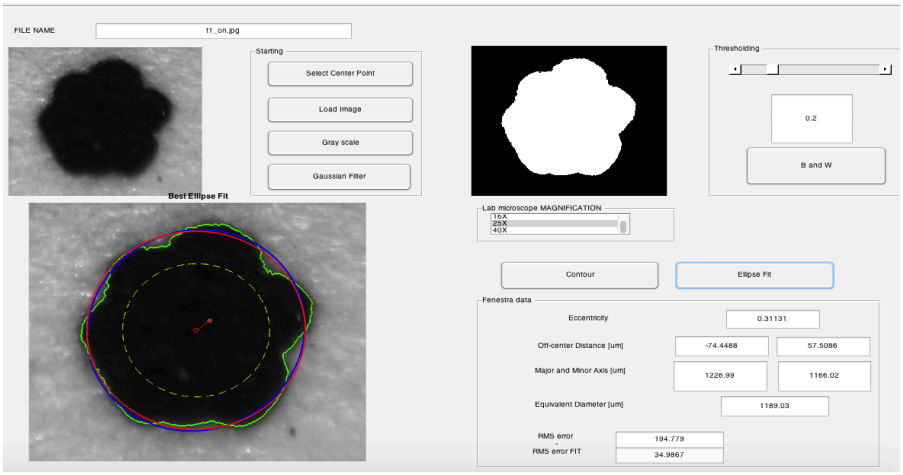

Fig. 6.4: Graphical User Interface developed for image processing of the photos taken to the rosettes after each trial. Image is first processed, and than some geometrical parameters are computed. Superimposed to the bottom black and white image, the green line is the rosette contour detected, the red line is the equivalent circle, the blue line the best ellipse fit, the yellow dotted line the ideal rosette and the red points are the centroid and the supposed center of the rosette.

- Aspect ratio

  This number is the ratio between the best fit ellipse major and minor axis. Aspect ratio equal one is a circle;
- Equivalent diameter

  This diameter is the one of a circle with the same area as the area inside the rosette contour;
- $RMS_{contour}$

  This error is computed as follow:

$$RMS_{contour} = \sqrt{\frac{\sum_{i=1}^{n}(r_i - r_{equiv})^2}{n}} \tag{5.13}$$

being r_i the radius of the *i-th* point of the rosette contour and r_{equiv} the radius of the equivalent circle, as can be seen in Fig. 6.5. n is the total number of points along the contour.

This is a measure of how smooth the rosette contour is. The bigger $RMS_{contour}$ the more irregular the rosette outline;

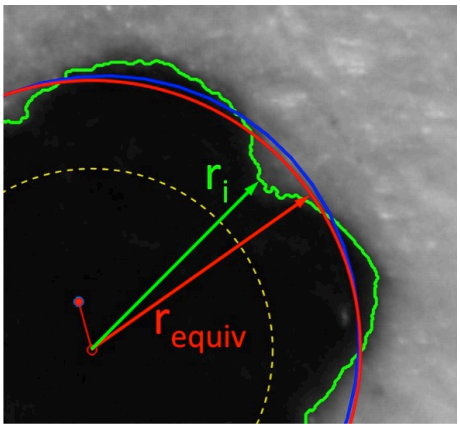

Fig. 6.5: Rosette contour detection and calculus of the RMS error, index of the irregularity of the rosette contour.

Other parameters important for the analysis were calculated using the data recorded with Micron during the trials. Those were:

- Saturation

  It indicates the percentage of Micron stacks saturation. When a motor is saturated, the cancellation is compromised because Micron cannot move "freely" the tip. Thus it is important to know when saturation occurs and the related effects;

- RMS_{tremor}

  The total motion can be divided in wanted and unwanted motion (tremor) as seen in chapter 4.1. The displacement due to the tremor along each direction was computed by filtering the total motion. Thus for every point of the trajectory the displacement d_i in 3D due to the tremor was computed. Then the RMS was computed to have an index that describes how much the tremor affects the tip trajectory.

This was computed as:

$$RMS_{tremor} = \sqrt{\frac{\sum_{i=1}^{n} d_i^2}{n}} \tag{5.14}$$

being d_i the amplitude of tremor in the *i-th* point along the trajectory (see Fig. 7.3) and n the total number of points. The tremor signal was deducted from the tip position signal by applying an ideal filter;

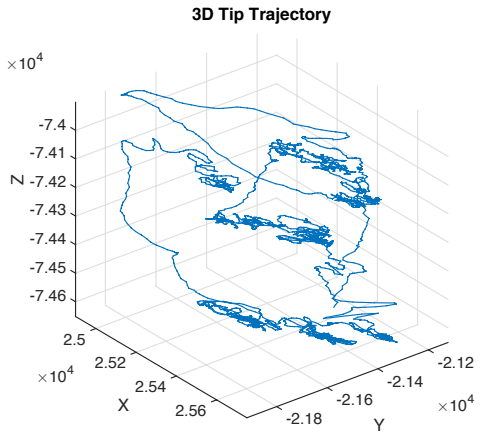

Fig. 6.6: Tip trajectory in the space while performing the rosette using the laser.

- Max_{tremor}

  This is the maximum 3D displacement due to tremor in each trial;

- Trajectory path

  It is possible, through some data analysis, to plot 3D, 2D or 1D tip, handle or goal positions for further data analysis.

Bone trials

Image processing on the images got from the bone trials were much more complicated than the one for paper trials. This is due to the different

environment surrounding the rosette: in the paper trials there was white plane paper, instead in the bone trials, cadaver's bones were used.

For bones images a *colour-based segmentation method using K-means clustering* was used [36]. This method consists on:

a) Read the image, by default in RGB (red green blue) color map;
b) Convert the image to *Lab color map*. As the RGB map, the *Lab* map is a tristimulus map. This color map has three axes: the a-axis goes form green to red, the b-axis goes from blue to yellow and the L-axis is the brightness. So the image is formed by a matrix with three layers corresponding to *L*, *a* and *b* axes;
c) Using the k-means clustering techniques pixels are grouped into clusters based on their color similarity: this is done using the Lab color map;
d) Each pixel is then labeled corresponding to its cluster;
e) Each cluster is plotted so the clusters making the rosette shape are separated to the ones in the surroundings;
f) The clusters making the rosette are grouped and an image is formed using only these clusters: the rosette can be seen excluding the background;
g) The contour of the rosette was then detected;
h) Having the contour of the rosette its geometrical properties can be computed and the centroid, the best ellipse fit, the equivalent area circle plotted (Fig. 6.7).

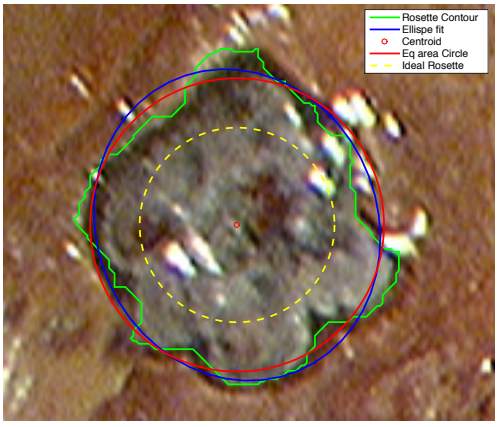

Fig. 6.7: Rosette contour detection (green), best fit ellipse (blue), equivalent area circle (red) and ideal rosette shape (yellow). This is the result of image analysis of bone trials.

Having these data the same parameters as the model trials were computed.

The ideal rosette is a circle with diameter of 800 μm [10]; its data are shown in Table 6.3:

Ideal rosette shape	Value
Eccentricity (-)	0
Aspect ratio (-)	1
Equivalent diameter (μm)	800
$RMS_{contour}$ (μm)	0

Table 6.3: Ideal rosette data: this is a circle with 800 μm diameter.

An ideal user would preform this task keeping the RMS_{tremor} and the Max_{tremor} displacement as low as possible and the trajectory should be a circular path with some hold still moments when the laser is fired.

During each trial photos and videos were recorded. Form this documentation it was possible to understand the completion time and if some anomaly occurred.

For each quantity are presented:

- Mean: mean value across all the trials;
- σ : standard deviation across all the trials;
- Max: maximum value across all the trials;
- Min: minimum across all the trials;

6.3.2 Depth measure

The aim of this measure was to detect how deep the tool tip went.

First, the plane that lies on the stapes footplate upper surface was determined. This plane was needed to compute the depth penetration, taking it as zero-plane. Second, the fenestraiting pick tip trajectory was analyzed during the fenestration, and the maximum depth was computed.

As mentioned in chapter 6.2 the depth measure begins with the user touching the stapes footplate, three times, going as straight as possible (*scan*): in Fig. 6.8 the tip trajectories while doing this movement can be seen.

From these data two important information were extracted:

- Normal vector perpendicular to the stapes footplate surface

  Processing and analyzing the tip trajectory, the normal vector to the stapes footplate surface was extracted, as can be seen in Fig. 6.8.

  Considering **M**, the $m\times3$ matrix of points of one scan, and using the *singular value decomposition (svd)*, the following factorization can be obtained:

$$\mathbf{M} = \mathbf{U} \cdot \mathbf{S} \cdot \mathbf{V}^T \tag{5.15}$$

  where **U** is an $m\times m$ unitary matrix, **S** $m\times3$ rectangular diagonal matrix and **V** is a 3×3 unitary matrix.

  The only interesting matrix here is **V**, since its columns are vectors of an orthonormal basis, from where the vector along the scan line is obtained.

  So for every scan a vector along its line was obtained:

$$\mathbf{n}_{scan\_i} = \begin{Bmatrix} u_i \\ v_i \\ w_i \end{Bmatrix} \tag{5.16}$$

  At this point the average of the $\mathbf{n}_{scan\_i}$ components formed the normal vector to the stapes footplate plane **n**:

$$\mathbf{n} = \begin{Bmatrix} \frac{1}{3}\sum_{i=1}^{3} u_i \\ \frac{1}{3}\sum_{i=1}^{3} v_i \\ \frac{1}{3}\sum_{i=1}^{3} w_i \end{Bmatrix} \tag{5.17}$$

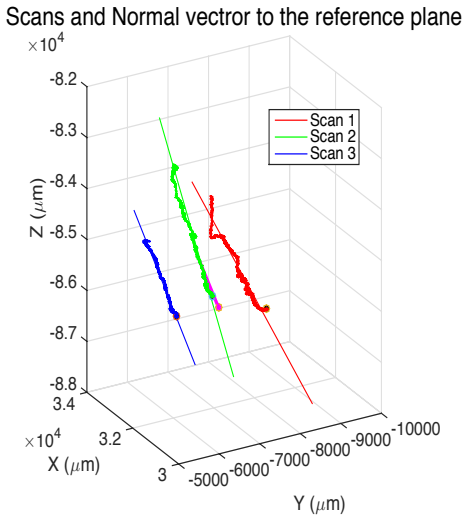

Fig. 6.8: Scans of the tip trajectory during the procedure to compute the normal vector to the stapes footplate surface. The normal vector **n** is in magenta. The three scans are as vertical as possible, but the reference system is the ASAP, so they appear with some angle according to the ASAP pose during the trial.

- Points on the stapes footplate upper surface

  The last point of each scan was taken as point lying on the stapes footplate upper surface:

$$P_i = (x_{P_i}, y_{P_i}, z_{P_i}) \tag{5.18}$$

  The point on the stapes footplate C was calculated as the average of the P_i points:

$$C = \left(\frac{1}{3}\sum_{i=1}^{3} x_{P_i}, \frac{1}{3}\sum_{i=1}^{3} y_{P_i}, \frac{1}{3}\sum_{i=1}^{3} z_{P_i} \right) \tag{5.19}$$

At this point, a normal vector **n** and a point on the stapes footplate plane *C* were defined: the reference zero-plane was defined.

Data were collected also during the fenestration procedure. Having all the tip position data throughout the procedure sampled at 2 kHz, the more distant point below the reference plane was detected: this is the depth measure.

Having the plane normal vector **n**, and by doing the dot product between the normal vector and the vector **v**, vector from the plane center *C* to each tip position *P*, the distance d_{depth} from the plane of each point was computed (Fig. 6.9):

$$d_{depth} = \mathbf{v} \cdot \mathbf{n} = v \cdot \cos(\vartheta) \tag{5.20}$$

ϑ being the angle between the two vectors and modulus of **n** equal to one.

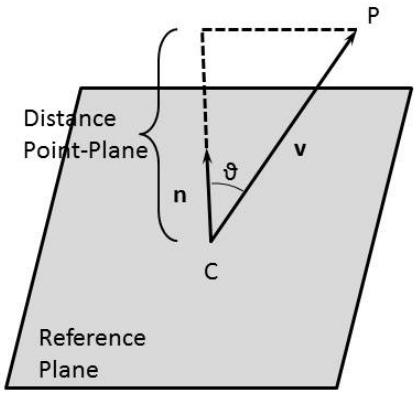

Fig. 6.9: Distance point - plane.

The maximum distance was taken to understand the depth penetration of the instrument and compare this measure in the aided and unaided case.

This depth calculation system produces an error on the measure because different scans give different results on the orientation of the normal vector **n** and points on the reference plane.

Taking in consideration that with different scans there is an angular discrepancy γ and a distance discrepancy d_{err}. The error on the distance e_d was computed as:

$$e_r = d_{err} \cdot \cos(\gamma) \tag{5.21}$$

7 Results

This chapter presents the results for both model and bone trials. Numerical data are presented through some tables and plots: first the geometrical data, then the tremor values, the effect that cancellation gives and, as last, the completion time. Comments and discussion of the results are done in chapter 8.

7.1 Rosette geometrical data

This section presents the geometrical data, resulted from image processing and data analysis. First the model trial results are presented and then the bone ones.

Fig. 7.1 displays a rosette done using the ear model. The stapes shape is in yellow, light color advantageous for the image processing. The stapes footplate was modeled with a piece of paper with a printed shape: this was a rectangle with smoothen edges (length: 3 mm, width: 2 mm).

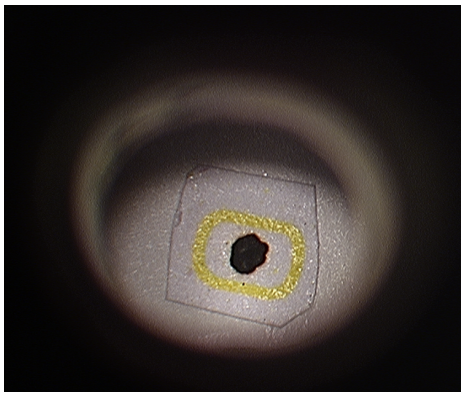

Fig. 7.1: Rosette performed during a model trial: the ear model was used as target. It can be seen the yellow shape that resembles the stapes footplate shape and the black rosette in the center performed by overlapping laser bursts.

In Table 7.1 and Table 7.2, the geometrical characterization of the rosettes shape in the model trials is reported. To notice that in the penultimate row of these two tables there are no values for the saturation, since Micron is off: the motors were not working and thus saturation could not happen.

Rosettes shape Model Trials (Surgeon 1)		Mean	σ	Max	Min
Eccentricity (-)	Off	0,40	0,12	0,57	0,26
	On	0,46	0,12	0,60	0,32
Aspect ratio (-)	Off	1,10	0,07	1,21	1,03
	On	1,14	0,08	1,25	1,05
Equivalent diameter (μm)	Off	1414,6	118,5	1595,2	1278,1
	On	1435,5	27,5	1455,2	1388,3
$RMS_{contour}$ (μm)	Off	50,7	10,1	60,0	33,7
	On	52,1	10,4	63,6	38,9
Saturation (%)	Off	-	-	-	-
	On	15,96	5,43	25,29	11,49

Table 7.1: Surgeon 1, rosettes geometrical results comparison in model trials: unaided vs. aided case.

From the table above, it can be noticed that the rosettes done by the first surgeon were slightly better in the unaided case: eccentricity and aspect ratio are lower, meaning a better circularity; lower $RMS_{contour}$ means that the contour was smoother. The aided result is not affected by saturation, since it is quite low (mean of 15,96%), so Micron was working well and cancelling the hand tremor most of the time.

On the other hand, the results for the second surgeon (Table 7.2) were better in the aided case, so with the help of Micron: eccentricity, aspect ratio and $RMS_{contour}$ are lower.

Therefore results are in contrast in for the two surgeons; this can be due to many factors that are discussed and listed in chapter 8

Rosette shape Model Trials (Surgeon 2)		Mean	σ	Max	Min
Eccentricity (-)	Off	0,41	0,17	0,57	0,16
	On	0,37	0,04	0,40	0,31
Aspect ratio (-)	Off	1,12	0,08	1,22	1,01
	On	1,08	0,02	1,09	1,05
Equivalent diameter (µm)	Off	1107,0	36,2	1138,7	1053,5
	On	1164,6	78,7	1250,1	1050,1
$RMS_{contour}$ (µm)	Off	35,2	9,1	45,4	24,3
	On	32,0	1,3	33,8	30,6
Saturation (%)	Off	-	-	-	-
	On	14,68	3,66	18,24	9,82

Table 7.2: Surgeon 2, rosette geometrical results comparison in model trials: unaided vs. aided.

Fig. 7.2 shows the fenestrations at the end of each bone trial, performed by the first and second surgeon respectively. Instead Table 7.3 and Table 7.4 present the geometrical results for bone trials.

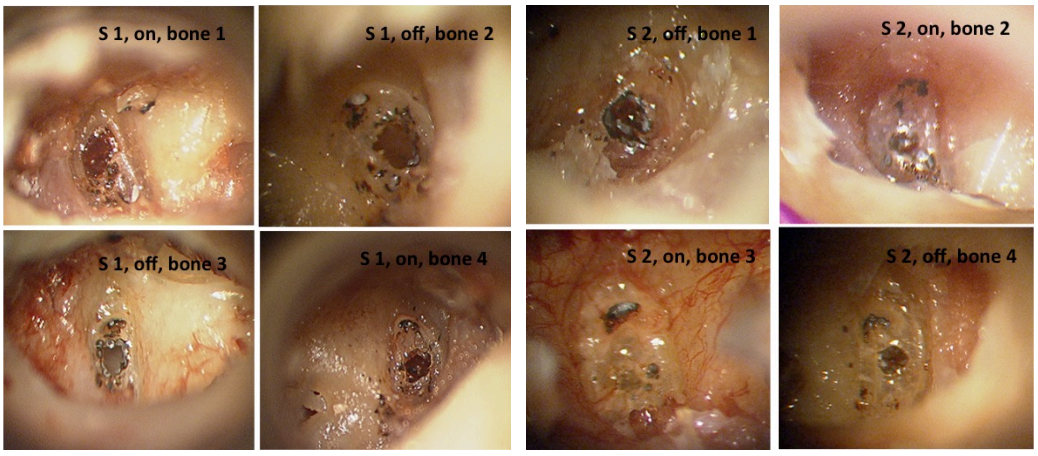

Fig. 7.2: Bone fenestrations, surgeon 1 (left) and surgeon 2 (right).

Rosettes shape Bone Trials (Surgeon 1)		Mean	σ	Max	Min
Eccentricity (-)	Off	0,59	0,09	0,66	0,53
	On	0,55	0,09	0,69	0,49
Aspect ratio (-)	Off	1,25	0,11	1,33	1,18
	On	1,20	0,08	1,26	1,15
Equivalent diameter (μm)	Off	911,1	33,8	934,9	887,2
	On	934,7	163,9	1050,7	818,7
$RMS_{contour}$ (μm)	Off	61,4	0,7	61,9	60,9
	On	47,7	14,5	58,0	37,5
Saturation (%)	Off	-	-	-	-
	On	33,3	18,7	46,5	20,0

Table 7.3: Surgeon 1, bone trials rosette geometrical results comparison: unaided versus aided.

Rosettes shape Bone Trials (Surgeon 2)		Mean	σ	Max	Min
Eccentricity (-)	Off	0,49	0,05	0,53	0,46
	On	0,48	0,14	0,58	0,37
Aspect ratio (-)	Off	1,15	0,03	1,18	1,13
	On	1,15	0,10	1,22	1,08
Equivalent diameter (μm)	Off	1003,4	287,1	1206,4	800,4
	On	586,9	172,4	708,4	465,0
$RMS_{contour}$ (μm)	Off	47,9	16,1	59,3	36,5
	On	25,4	6,0	29,7	21,2
Saturation (%)	Off	-	-	-	-
	On	13,4	1,0	14,1	12,7

Table 7.4: Surgeon 2, bone trials rosette geometrical results comparison: unaided versus aided.

To notice that on the top left square (S1, on, bone 1) of Fig. 7.2, the fenestration has a shape that is not really circular. This is because the stapes footplate was already fractured, and when the surgeon used the fenestrating pick, it broke down.

It can be seen that the environment in the bone trails is totally different if compared to the model trials: many uncontrolled variables (like left/right ear, condition of the footplate and small fractures) are added, and the operations become harder.

In the bone trials the eccentricity is lower in the robot-aided case for both the surgeon: Micron seems to help performing the rosette shapes more circular. Also the $RMS_{contour}$ is lower (-23% for surgeon 1 and -47% for surgeon 2) and consequently the rosette contour is more smooth and regular.

7.2 Tremor reduction

The effect of cancelation can be seen in the Fig. 7.3 where the tip motion is plotted and filtered to distinguish different motion components: tip actual motion, wanted hand motion and hand tremor (disturbance).

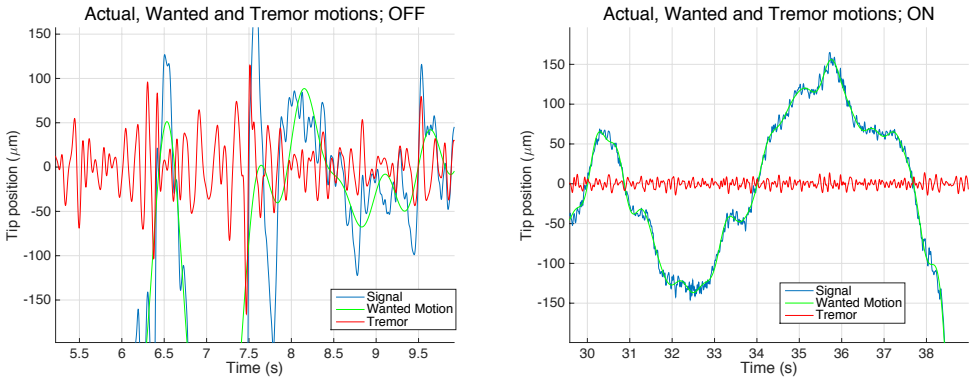

Fig. 7.3: Tremor cancellation effect: cancellation off (unaided case) (left) and cancellation on (aided case) (right). The wanted motion (green) is the actual motion (blue) minus the tremor (red).

The aided case presents a much lower tremor amplitude compare to the unaided case due to the effect of Micron tremor cancellation. Table 7.5 presents the tremor data of the model trials:

Tremor Model Trials		RMS_{tremor} (μm)				Max_{tremor} displacement (μm)			
		Mean	σ	Max	Min	Mean	σ	Max	Min
Surgeon 1	Off	19,9	2,2	22,4	18,0	101,6	18,0	133,3	87,8
	On	8,7	0,9	9,8	7,5	87,2	38,1	143,7	54,7
Surgeon 2	Off	26,4	3,0	29,8	22,9	89,1	6,2	95,4	81,0
	On	7,2	0,9	8,5	6,3	26,4	9,4	42,8	19,9

Table 7.5: RMS_{tremor} and Max_{tremor} displacement of the tremor during the rosette task in model trials.

It can be seen that Micron helped to reduce tremor in the model trials: the RMS_{tremor} is reduced 56% for the first surgeon and 72% for the second one. Also the max error is reduced significantly.

Tremor Bone Trials		RMS_{tremor} (μm)				Max_{tremor} displacement (μm)			
		Mean	σ	Max	Min	Mean	σ	Max	Min
Surgeon 1	Off	31,7	6,0	36,0	27,4	162,8	46,6	195,4	130,1
	On	18,5	1,3	19,4	17,5	266,6	77,3	171,9	281,2
Surgeon 2	Off	45,3	2,1	46,8	43,8	287,5	83,7	346,6	228,3
	On	18,9	4,6	22,2	15,7	211,4	89,4	274,6	148,2

Table 7.6: RMS_{tremor} and Max_{tremor} displacement of the tremor during the rosette task in bone trials.

The tremor is reduced in the bone trials too, 42% for surgeon one and 58% for surgeon two.

An interesting thing to notice is the max tremor displacement. Only for surgeon one in bone trials there is a max error due to tremor with Micron on that is bigger than for the off case. This can happen because if the motion on the hand is too quick or sudden, Micron tries to recover the null-tip position moving fast the tip: this produces a jerk and so a big displacement error.

7.2.1 Tremor cancellation effect

Another effect of cancellation can be seen in Fig. 7.4 where tip actual position, goal position and null tip position are shown.

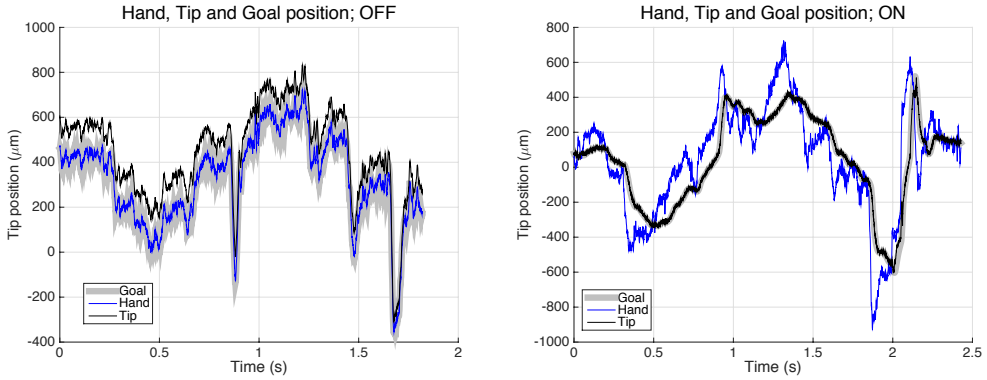

Fig. 7.4: Hand, goal and tip position comparison unaided (left) versus aided (right) case.

The goal position filter, applied to keep wanted motion and reject tremor, introduces also a delay. This delayed motion is not present obviously in the unaided case, since Micron is not on, and so no goal filter is applied.

It can be also noticed that in the aided case the tip follows quite well the goal position, which means Micron control is working well.

Fig. 7.5 shows the effect of cancellation on the trajectory of the laser probe tip while performing the rosette. Form this figure it can be seen that the path is much more regular and circular in the aided case where the tremor cancellation is on. This is because in the aided case the tremor is cancelled and so only the voluntary motion of the surgeon drives the tool tip.

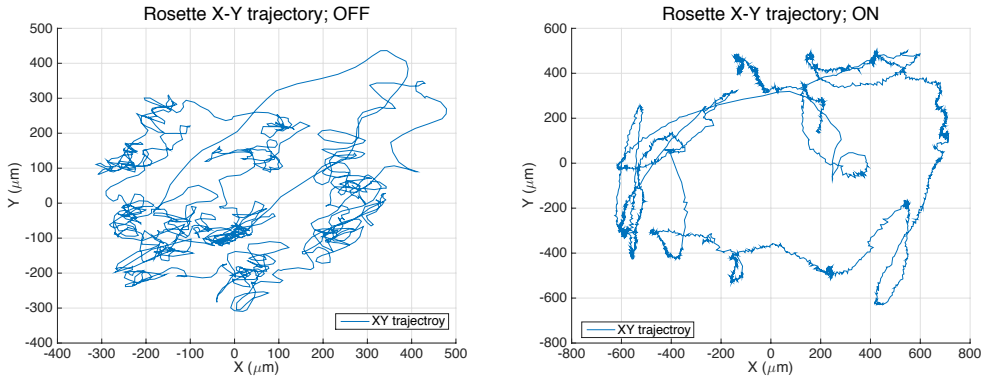

Fig. 7.5: 2D trajectory while performing the rosette comparison: unaided (left) versus aided (right).

It can be noticed from the previous figure that the aided signal is noisier: this is due to the fact that control loop is working, electrical signal is flowing and noise is a component of this signal: it has really high frequency and thus is not affecting the performance.

7.3 Depth penetration measure

This measure was possible only in the bone trials. It can be noticed how the standard deviation is really high; this is because the trails were only two on and two off for each surgeon.

Bones Depth penetration (μm)		Mean	σ	Error
Surgeon 1	Off	-731	199	±56
	On	-808	291	±40
Surgeon 2	Off	-680	53	±98
	On	-752	66	±151

Table 7.7: Depth penetration results in bone trials. The zero-plane and the error are defined in chapter 6.3.2.

The error on the measure was calculated as the mean of the error of every trial: this error takes into account the angle of the different scans used to compute the normal vector **n** and the error position of the plane point *C* (see chapter 6.3.2). These two variables influence the reference plane definition and so the depth measure.

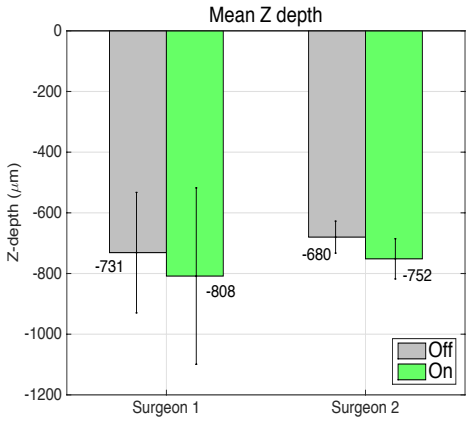

Fig. 7.6: Mean Z depth penetration during bone trials. σ is reported as a vertical line for each bar.

Fig. 7.6 presents the penetration depth while performing the opening on the stapes footplate using the fenestrating pick. It is better to keep the penetration depth as low as possible to avoid touching, and so hurting, delicate tissues under the footplate.

The zero-plane taken as reference is the upper surface of the stapes footplate.

It can be seen that both surgeons had gone less deep in the unaided case, so with Micron off. But in this case it is hard to state a conclusion since the depth penetration measure is affected by an important error and the trials were too few to state something.

7.4 Rosette completion time

As it can be seen from Table 7.8, the rosette completion time is a bit bigger in the aided case. This was expected since Micron needs to be moved slowly to avoid saturation of the instrument and also because surgeons are much more trained with Micron off: it is like a common surgical instrument.

Trials Completion time (s)		Mean	σ	Max	Min
Surgeon 1	Off	23,6	3,4	29	21
	On	27,2	1,6	29	26
Surgeon 2	Off	19,2	3,5	25	16
	On	21,2	2,2	23	18

Table 7.8: Model trials rosette completion time.

The values in the previous table are in seconds. Even if the completion time was greater in the aided case, it would not affect the surgery outcomes. And since the difference is few seconds, it does not create a problem of time expense in the OR.

The completion time for the bone trials are not shown: this variable was affected by the anatomy of the stapes footplate. In fact the number of bursts needed is related to the thickness of the footplate, and this variable could not be controlled: the ticker the bone the longer the completion time.

Moreover, in some trials the rosette was performed and after that, the surgeon needed the laser another time to lower the thickness of the footplate before working with the fenestrating pick.

7.5 Statistical Analysis

To understand how robust the results obtained are, statistical significance calculations were done.

Since the data population was small, the decision to group all data in *on* and *off* case was taken, regardless of which surgeon or trial. This means that only the statistical significance between Micron aided and unaided case is sought.

In Table 7.5 and Table 7.6 mean, standard deviation, max and min tremor results are shown for the model and bone trials respectively and separately. In this section, for the statistical analysis, all the trials data (so five model sessions and two bone sessions) are grouped and a new average and standard deviation are calculated, based on all data group together. The same was done for the geometrical data presented separately in Table 7.1- Table 7.4 and here grouped together.

The average, standard deviation, max and min of this grouping can be seen in Table 7.9 and Table 7.10. Plots are shown in Fig. 7.7 and Fig. 7.8. The main reason for that was having an *on* and *off* groups big enough for the statistical tests.

It can be immediately seen that the eccentricity and $RMS_{contour}$ are close to each other and with high standard deviation, while the difference due to Micron on use for the RMS_{tremor} and Max_{tremor} seems more consistent.

Rosette Shape (All trials)		Mean	σ	Max	Min
Eccentricity (-)	Off	0,45	0,14	0,66	0,16
	On	0,44	0,10	0,61	0,31
$RMS_{contour}$ (μm)	Off	46,6	12,9	61,9	24,2
	On	40,5	13,2	63,6	21,2

Table 7.9: Eccentricity and $RMS_{contour}$ computed grouping all the trials.

Tremor (All trials)		Mean	σ	Max	Min
RMS_{tremor} (μm)	Off	27,5	9,0	46,8	18,0
	On	11,0	5,3	22,2	6,3
Max_{tremor} (μm)	Off	132,5	75,8	346,6	81,0
	On	103,2	89,8	281,2	19,9

Table 7.10: RMS_{tremor} and Max_{tremor} computed grouping all the trials.

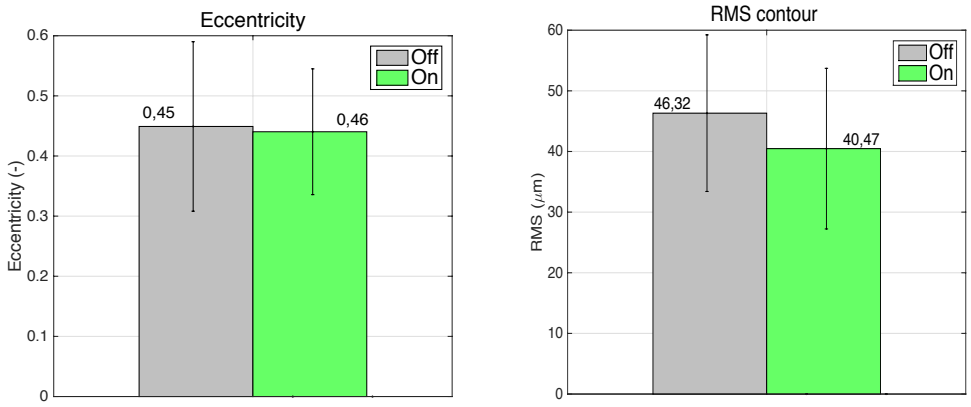

Fig. 7.7: Geometrical data of all the trials: mean *e* (left) and $RMS_{contour}$ (right). σ is reported as a vertical line for each bar.

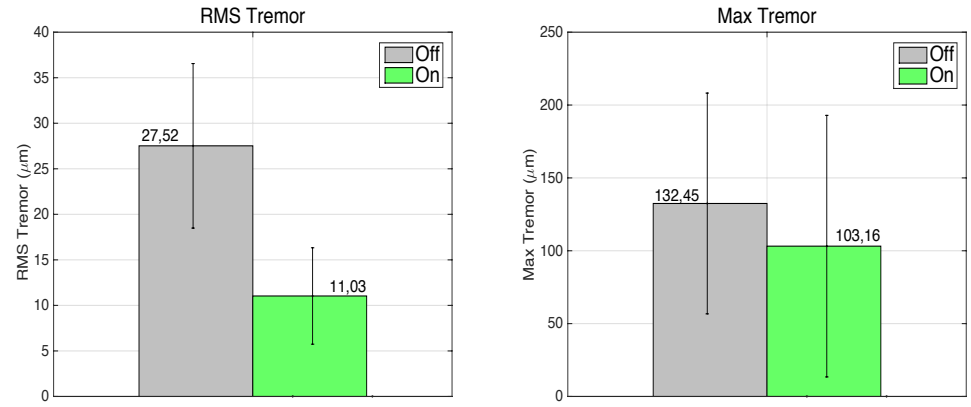

Fig. 7.8: Tremor data of all the trials: RMS_{tremor} (left) and Max_{tremor} (right). σ is reported as a vertical line for each bar.

Since the population is small and the distribution unknown, non-parametric statistical tests must be used. Non-parametric tests do not rely on parameters estimated form the distribution [37], since it is unknown.

It is always desirable to use more than one-non parametric test and compare the results because each non-parametric test has its own weakness.

Being in this situation, the tests used to see if statistical significance was reached were:

- Kolmogorov-Smirnov (KS) two-sample test, non-parametric alternative to the Student t-test;
- Kruskal-Wallis (KW) test that is the non-parametric alternative to ANOVA.

p-values obtained form these tests are reported in Table 7.11.

p-value (All trials)	KS test	KW test
Eccentricity	0,54	0,71
$RMS_{contour}$	0,26	0,21
RMS_{tremor}	0,00018	0,00028
Max_{tremor}	0,03	0,06

Table 7.11: *p*-values from the nonparametric statistical KS and KW tests: the statistical significance between Micron on and off was tested. The significance level was 0,05.

It can be seen that both tests gave no statistical significance ($p > 0,05$) for the small improvement of rosette shape, due to the aid of Micron. In Fig. 7.7 in fact the difference between on and off case is small and the σ is large in both plots.

Better results were obtained for the tremor reduction: statistical significance was reached for the RMS_{tremor} reduction ($p < 0,05$): both tests confirmed it. In the left plot of Fig. 7.8, σ is not small, but the mean values difference is large.

For the Max_{tremor} reduction the two tests give a contrasting results: the KS test result is 0,03, so statistical significance is reached ($p < 0,05$); the KW test gives

the opposite result, since $p > 0{,}05$. So for the Max_{tremor} reduction contrasting results are obtained. In fact analyzing Fig. 7.8, right plot, it can be seen that the mean difference is not so high, and the standard deviation is large too: thus the claim of statistical significance seems not convincing.

8 Discussion

After the design and tools manufacturing for Micron in middle ear microsurgery, test where performed using an ear model, and simulating more real conditions, using temporal bones form cadavers.

Trials were designed to test surgeons' performances in the robotic aided and unaided case. Data where recorded during the trials and analyzed thoroughly to have a deep understanding on the results. In chapter 7, geometrical results, tremor cancellation effects, depth measure and completion time are exposed.

In this chapter the results are discuss analyzing some possible causes:

- *Surgeon experience level and training*

The geometrical data results obtained by the two surgeons in the model trials, were different: the first surgeon had better results in terms of rosette shape in the unaided case, while the second surgeon did better with Micron on. In the bone trials instead, both surgeons performed slightly better rosettes in the robot-aided case.

This difference can be due to the level of surgeon's experience and also the training that each surgeon had with Micron on: the learning curve depends on the subject. Some pre-trials were done to test and set the experiment setup: rosettes performed were totally better in the unaided case. But already in the next experiments, the one presented here, the results improved. So the amount of training is a main factor that affects the outcomes.

Due to the lack of time and surgeons' availability, more trials could not be done, but this result suggests that performances get better if surgeons have more "hands on" experience with Micron. This fact is promising.

- *Controlled motion and tiredness*

The other aspect to consider was the time of the day when the trials were performed. This variable unfortunately could not be controlled: experiments

were done according to surgeons' schedule. Sessions were done usually in the evening, after the end of the surgeons' working day, some others, but only with the second surgeon, in the early morning. This aspect is quite important, since at the end of the day, the level of tiredness and fatigue is totally different compared to the morning. Of course a more "fresh" surgeon performs better than a tired one.

Micron needs concentration to obtain good results and advantages from tremor cancellation: the motion should be slow, otherwise motors saturate due to the limited workspace, and cancellation is compromised. In this situation Micron becomes worse than a conventional instrument, because the actuated tip tries to recover the motion, but since the amplitude of the movement is too wide, the tip is moved rapidly and spasmodically around, the user looses the eye-hand coordination and the performance worsen.

- *Bone trials: uncontrolled variations*

In bone trials even more uncontrolled variables were introduced: the condition of cadaver's bones were not a negligible aspect. In one case the stapes footplate was already fractured (bone 1, surgeon 1, Fig. 7.2), so not fixed and at the end, an entire part of footplate came out.

Significant to consider is also the big difference between alive and cadaver's tissue: the latter one is more fragile and stiff compared to the former one. Moreover the bones used were not from humans with otosclerosis, so the stapes footplate was not fixed; it was slightly floating due to the wet tissue around. This meant that the working conditions for the surgeons were harder, since the fenestration had to be done on a floating surface rather than a fixed one.

- *Tremor reduction and use of the speculum*

Tremor amplitude reduction was significantly lower in the aided case: this lead to a better and more efficient trajectory path to accomplish the rosette bursts in a circular shape. Reduced tremor amplitude and optimized trajectory leads to a safer and more precise tool motion, preventing erroneous contacts with surrounding tissue that can lead to complications during surgery. But there was not a big difference on the quality of the rosettes.

The reason why there was not a big difference on geometrical results can be the speculum support.

Micron is an instrument capable of cancelling the hand tremor: it is efficient and effective if tremor heavily affects the performance, which means when tremor amplitude has the same order of magnitude as the task performed.

In middle ear surgery, surgeons are helped by the speculum, surface against which tools can be rested to lower hand fatigue and reduce tremor. Surgeons are trained to do that, and therefore, for them, pushing the tool against the speculum is the more natural thing to do. For that reason the brace was done, to prevent the tool to touch the speculum, leading to saturation. But there is a trade-off: if the brace is more "protective", helping to avoid saturation, it also creates more view obstruction. This happens because the tool, in order not to touch the speculum, needs to be more distant from it, more towards its center and thus more in the visual field.

Using the speculum, surgeons already reduce their hand tremor: in this way Micron is less effective, since tremor is already reduced.

During the trials, surgeons were posing the brace against the speculum, trying to avoid to block or saturate the actuated tip while Micron was on. Instead, while Micron was off, the tremor was reduced in their conventional way, by resting the tip against the speculum: in the unaided case they could not feel when the tip touched the speculum. In aided and unaided cases, tremor was reduced in some way; this is probably the main reason why the geometrical results are similar in both cases.

Likewise, analyzing the max tremor displacement can be seen that its values are much smaller compared to the task size: the rosette size should be around 800 μm, instead the max tremor displacement in the worst (off) case is less than 15% of the task measure. So the disturbance given by the tremor, already lowered by resting against the speculum, is not heavily affecting the task performance.

- *Depth penetration measure*

Depth penetration measure was calculated to check if there was difference between aided and unaided case. This was done only for the bone trials, during the last step, when surgeons worked with the fenestrating pick to remove the bony part inside the fenestra, and obtain a hole in the footplate. How deep the

surgeon goes depends also from the thickness of the footplate. This operation is the most delicate of the whole stapedotomy procedure, for the risk of touching the delicate vestibular tissue under the stapes footplate that can lead to bad consequences.

The results are affected by the error due to the reference plane definition and the accuracy of the ASAP system detecting Micron position. The angle and the last point of the scans are fundamental to define the normal vector, reference point and thus the reference plane. Another error that influences this measure derives from the calibration: errors in the calibration procedures are reflected in the ASAP pose detection accuracy, and thus in the position measure.

These measures do not differ much between aided and unaided case: more trials are needed to reach statistical significance and understand if Micron can really affect how deep the tool goes.

Important to observe that this operation is performed in a setting in which the depth perception is really hard: the tool is almost vertical, constrained from the speculum, the illumination is not excellent due to the speculum, so surgeons cannot rely on shadows to understand if they are close or not to a surface.

Binocular microscope can help somehow to have the depth perception, but its effect is not strong.

8.1 Surgeons' opinion

Since Micron is still under development, one important opinion after the experiments derives form the surgeons that are the final users. How was their feeling and the overall opinion is fundamental to assess the system from the user perspective and draw ideas for future improvement and development.

Cons highlighted were the following:

- Concern about the calibration process

  In the trials done only few steps of stapedotomy were performed, but in real operations many tools need to be used. To obtain an optimal tremor cancellation every time the tip should be changed.

This requires a system that allows changing the tips and doing the calibration really quickly;

- Hindering of natural motion

  Sometimes the device was correcting the position of the surgical instrument creating wide excursions detrimental for the process. However this is due to saturation;

- Line of sight obstruction and speculum as resting point;

  If the tip touches the speculum, saturation occurs. So the brace was done, but also the user should pay attention while using Micron. This fact has two consequences: view obstruction since the tool is moved more towards the center of the speculum and hand fatigue since the speculum is a support were to rest the tip;

Pros are fundamental too, so strong characteristics of Micron are acknowledged:

- Potential to control fine movements to minimize undesired excursions

  With Micron high positioning accuracy can be reached. This is a clear advantage given by Micron and it is useful especially in surgical steps that require fine and precise movements;

- Micron can be used in many surgical fields

  In otologic surgery Micron can be used for all the operations that involve the stapes, to correct otosclerosis or other diseases like cholesteatoma.

  Further applications are in middle ear surgery where often the speculum is not used, avoiding all the limitation that it creates using Micron and so having more freedom of motion for Micron.

  Ophthalmologic surgery is another field of possible applications: there is no speculum and more freedom of orientation and motion.

8.2 Future improvements

What can be done to ride over the problems discussed above?

- System for a quick instrument change

  It can be implemented for instance using a fast male-female coupling. One requirement is to keep the coupling system as small as possible to avoid view obstruction or to keep the connection out of the line of sight;

- More training for the user to understand how Micron behaves

  At first using Micron is not easy. Its motors introduce a motion of the tip that requires training to be fully understood and consequently used optimally. If the user has not enough training the tip motion sometimes appears strange and unnatural.

- Motors working independently when saturation occurs

  Surgeons are trained with conventional surgical tool. They rest the tool against the speculum and this gives three advantages: the tool is on the side so no view obstruction, it is a method to limit the hand tremor and it reduces the hand fatigue.

  It would be great to develop motors and software that allows the tip to be rested against the speculum also with Micron on. For instance if one motor is saturated the other two should continue to work to cancel the tremor as well as possible. In this way the surgeon could really use Micron as a normal tool with all the advantages that Micron provides, not caring where the tip is.

  A small hint can come also from a sound signal to alert the user when he/she is saturating the instrument.

Micron can be improved to reach even better results in otologic surgery. These possible improvements are:

a) Replace the optical tracker with a system that does not need a clear line

   During the experiment session one big problem was the PSD cameras positioning to put the LEDs inside the detected space.

This operation required long time because Micron had to be kept quite in the same position all the time, due to the limited detected space by the cameras.
If a system, which does not need a clear line could be developed, the advantage would be unquestionable. Anther related improvement could be to have a bigger detected space, so the surgeon is free to move the instrument without caring about Micron position and orientation.

b) Modify the brace or the tool to give a clearer view

To avoid saturation the brace keeps the tool in a position that was obstructing the view from the right eyepiece of the microscope. The component that was mainly disturbing was the connector, since it has a larger diameter compared to the instrument tip; it was though necessary to rotate the tool. If the connector could be done smaller, or the tool system changed, with an eye on the surgeon requirements, to lower the view obstruction, this can be a clear advantage for surgeons, who will have more visual control.

c) Perform more experiments in order to reach statistical significance and have a better assessment of the system

The number of trials done using cadavers' bone was really limited. To simulate the real surgical conditions, human bones are the best way. Models can help surgeons for the training phase, but for a better system assessment more bone trials are needed, so that statistical significance can be reached.

9 Conclusion

This thesis work demonstrates the design, manufacturing, tuning and testing of Micron, a fully handheld micromanipulator, in otologic microsurgery.

After a first study of the stapedotomy procedure, two tools were developed: a fenestrating pick and a laser probe. To use these tools, a brace was needed to prevent saturation and give a resting point to the user. To improve the ergonomic and the grip, a new handle was made.

After these changes, the control was configured to obtain an optimal cancellation. The process of system identification helped to find a model to simulate Micron dynamical behavior and develop a filter to have a good overall dynamic response.

Successively, experiments were done to assess the system performance and understand which improvements can be done. After the experiment design, some trials using an ear model first and cadavers' temporal bone then, were completed.

Data form the experiments were analyzed through image and data processing; results were displayed and commented.

From the results of this *pilot study* it can be concluded that:

- Micron helps more less experienced surgeons: the young surgeon did better with Micron on, the more experienced surgeon data shows the opposite;
- The completion time increases, but this is just few seconds, not creating problems of timing in the OR;
- Tremor reduction and the more efficient trajectory give a better control on the tip motion: this reduces the probability to touch delicate tissues during the surgery and thus avoid complications;
- Training "hands on" is important: Micron affects the human feedback loop control; the user needs to understand how Micron "behaves" and the slow and controlled motion that is needed with

Micron to obtain an optimal tremor cancellation. This is why tiredness is a relevant factor;

- The use of Micron affects the way surgeons operate: they usually rest and push the instrument against the speculum, but this cannot be done with Micron since in this case saturation will occur. This is another reason why training with Micron is really important.

It would be great to assess the influence of the training in the experiment outcomes: unfortunately there was not enough time and resources to do it during this research.

Results obtained with Micron, the fully handheld tremor cancelling system, are promising, but further development and improvement need to be done to reach clearer advantages in otologic surgery.

10 Riepilogo e Conclusioni *(in italiano)*

In questa sezione è fatto un breve riassunto del lavoro di tesi in lingua italiana. Il testo principale è interamente sviluppato nei capitoli precedenti in lingua inglese. Prego di riferirsi ai capitoli precedenti per spiegazioni esaustive del lavoro svolto, essendo riportato di seguito solamente un riassunto.

Introduzione

Questo lavoro di tesi è basato sullo sviluppo di Micron, sistema robotico realizzato per aumentare la precisione e controllo della manipolazione in microchirurgia, attraverso la cancellazione del tremore della mano. In particolare tale strumento-attivo è stato adattato alla stapedotomia, operazione di microchirurgia all'orecchio medio, che mira al ripristino dell'udito quando il paziente è affetto da otosclerosi.

Background Medico

L'orecchio umano è convenzionalmente diviso in tre parti: orecchio esterno, medio e interno (Fig. 2.1). Ai fini di questa ricerca, la parte importante da considerare è l'orecchio medio, dove si trovano la staffa (Fig. 2.3), incudine e martello (Fig. 2.2), tre piccoli ossicini che trasmettono e amplificano la vibrazione del suono dal timpano alle strutture presenti nell'orecchio interno.

L'otosclerosi (capitolo 2.2) è un'escrescenza ossea anormale (Fig. 2.4), solitamente sulla staffa, che blocca la normale vibrazione di questa catena di ossicini, provocando di conseguenza un deficit uditivo.

Una soluzione a questo problema si raggiunge attraverso l'operazione chirurgica denominata *stapedotomia* (capitolo 2.3). Essa ha come obiettivo il rimpiazzamento della staffa immobilizzata con una protesi a pistone. Dopo aver esposto la staffa, mediante bruciature laser si esegue una rosetta (forma circolare) sulla base della staffa (Fig. 2.5). La parte ossea viene quindi indebolita e successivamente con uno strumento appuntito un'apertura viene effettuata: in

questa apertura di forma idealmente circolare viene inserita la parte cilindrica della protesi-pistone (Fig. 2.6). La parte superiore della staffa è quindi sostituita da una protesi ed la normale vibrazione è restaurata, permettendo al paziente di recuperare l'udito.

Tassonomia dei robot per la chirurgia

I sistemi usati in robotica chirurgica possono essere suddivisi in tre categorie:

- Master/slave (capitolo 3.1.1)

  Questi sistemi robotici sono composti di due parti: console di comando (master) e braccia robotiche (slave) che eseguono le operazioni. Sono solitamente sistemi complessi e richiedono una procedura e un team dedicati;

- Cooperativi (capitolo 3.1.2)

  In questi robot il controllo dell'end-effector è suddiviso tra utente e robot, quindi si crea una sorta di cooperazione. Lo strumento è impugnato dall'utente e montato sul robot, che quindi percepisce le forze applicate dall'utente e le forze di reazione dall'ambiente. Questi dati poi sono processati dal controllo per aumentare le performance: cancellare il tremore, migliorare l'accuratezza, scalare il movimento, etc.

- Strumenti attivi (capitolo 3.1.3)

  Questo tipo di sistemi sono meglio descritti come "strumenti attivi" piuttosto che come robot. Infatti, l'utente li impugna come se fossero dei normali strumenti chirurgici, con la differenza che nell'impugnatura è presente il sistema di attuazione. Non sono quindi rigidamente connessi al terreno e non è presente alcun braccio robotico (Fig. 3.5 - Fig. 3.10).

Questa tesi è incentrata su Micron, uno strumento attivo, che appartiene alla terza categoria. Di conseguenza l'attenzione d'ora in poi sarà posta su tale tipologia di robot.

Un confronto tra i tre tipi di sistemi robotici è fatta al capitolo 3.2.

Micron: hardware e software

Prima di introdurre e descrivere Micron, è importante dare la definizione di tremore: qualsiasi movimento involontario della mano, indifferentemente a bassa o alta frequenza (capitolo 4.1).

Il principio che sta dietro a Micron è il seguente: i motori, nella parte attiva, si muovono in modo uguale e contrario al tremore dell'utente, di conseguenza cancellandolo. Dunque l'end-effector risulta stabile ed il suo moto in accordo con il movimento della sola componente volontaria della mano dell'utente.

Il sistema Micron è formato da tre componenti principali (Fig. 4.2):

1. Strumento (Micron)

   Lo strumento attivo (o Micron) è composto da un'impugnatura, una parte attiva che contiene tre motori piezoelettrici disposti in configurazione parallela e quattro LED, ed un end-effector che può essere cambiato a seconda della necessità del chirurgo (Fig. 4.3);

2. Apparatus to Sense the Accuracy of Position (ASAP)

   Questo sistema permette di rilevare la posizione dello strumento in sei gradi di libertà, con una precisione dichiarata di 4 μm. I principali elementi sono due sensori che rilevano la posizione delle quattro luci LED presenti sullo strumento. Tre luci sono montate sulla parte mobile e una sulla base. Questo permette di rilevare sia la posizione della parte mobile, che la posizione dell'impugnatura fissata alla base;

3. Elettronica

   La parte elettronica consiste in una macchina nella quale è implementato il controllo feedback in real-time. L'input è la posizione dello strumento attivo, mentre l'output sono le posizioni dei motori.

   Per controllare il sistema sono state sviluppate delle interfacce in LabVIEW che l'utente usa da un normale computer.

C’è inoltre un pedale che permette all’utente di cambiare modalità di funzionamento durante l’uso di Micron.

La parte software è interamente implementata in LabVIEW. Il sistema di coordinate usato, l’influenza di Micron sull’umano, il filtro che blocca la componente di tremore, il controllore ed il ciclo di controllo sono descritti nel capitolo 4.3

Materiali e metodi

Per prima cosa è stato sviluppato un modello per testare la strumentazione e capire di fronte a che scenario si trovano i chirurghi al momento della stapedotomia (capitolo 5.1). Il modello (Fig. 5.2) è stato realizzato con:

- *Speculum*: parte metallica a forma d’imbuto che è inserita nel canale auricolare del paziente durante l’operazione chirurgica;
- Tubo di plastica per simulare il canale auricolare;
- Modello di carta di spessore adeguato per simulare la base della staffa.

Del materiale plastico, colla e adesivo sono stati usati per mantenere in posizione le componenti sopra descritte.

Per le fasi della stapedotomia presa in considerazione, sono necessari due strumenti: uno appuntito con una leggera piega alla fine (“fenestraiting pick” in inglese) (Fig. 5.8) e un laser (Fig. 5.9). Entrambi gli strumenti sono stati realizzati partendo da richieste da parte del chirurgo (capitolo 5.2.1): trasformate le richieste in requisiti tecnici, si sono poi sviluppati i due strumenti necessari (capitolo 5.2.2).

Dopo aver realizzato gli strumenti, c’è stata la prova degli stessi. Dalla prova è risultato il problema della saturazione dei motori: ciò significa che i tre motori piezoelettrici di Micron non sono liberi di muoversi, ma c’è qualche impedimento che blocca uno o più di essi. Il problema s’incontra quando l’utente posa la punta contro il bordo dello speculum. Altro caso in cui la saturazione può avvenire è quando l’utente muove lo strumento troppo velocemente e Micron non riesce a correggere il tremore perché il range di movimento dei motori è limitato: il motore raggiunge il fine corsa e risulta in stato di saturazione.

Tale problema si è risolto tramite due accorgimenti: sviluppando una protezione che impedisse allo strumento di toccare il bordo (capitolo 5.3), e considerando che la possibilità di movimento dello strumento all'interno dello stretto canale auricolare è limitata.

Avendo eseguito dei test per l'ergonomia con il chirurgo in precedenza, si era deciso di migliorare la presa dello strumento sviluppando un'impugnatura più ergonomica. La nuova impugnatura sviluppata è più stretta, allungata, con una distribuzione migliore dei pesi avendo come effetto uno strumento più bilanciato (capitolo 5.4).

Quando nuovi strumenti sono montati su Micron, il sistema cambia dal punto di vista dinamico: ogni strumento, infatti, ha forma, materiali e inerzie differenti. Di conseguenza i parametri del controllo devono essere adattati per ottenere una cancellazione ottimale del tremore. Si è proceduto quindi con le calibrazioni necessarie e con l'identificazione dinamica del sistema che ha permesso di ottenere un modello dinamico del sistema (capitoli 5.5.1 - 5.5.2).

Esperimenti

Gli esperimenti hanno avuto l'obiettivo di comparare le prestazioni nei casi Micron on e Micron off. Quando Micron è disattivo, è come usare uno strumento convenzionale, non attivo. Così facendo si è potuto valutare se e quali vantaggi conseguono dall'uso di Micron e conseguente cancellazione del tremore.

I primi esperimenti sono stati svolti usando il modello di orecchio sviluppato, cosicché i chirurgi potessero prendere confidenza con lo strumento, capirne il funzionamento e conoscere le fasi dell'esperimento. In seguito si è passati alla sperimentazione su ossa da cadavere per simulare al meglio la reale situazione chirurgica.

Nel capitolo 6.1 è descritto l'ordine degli esperimenti ed i soggetti: due chirurgi specializzati nella stapedotomia, ma con diverso livello di esperienza.

L'obiettivo degli esperimenti è stato eseguire una rosetta di forma circolare sulla base della staffa, sovrapponendo bruciature laser, per poi eseguire un'apertura usando lo strumento di forma appuntita. Il design degli esperimenti e le fasi sono descritti nel capitolo 6.2.

Le misure effettuate per determinare le caratteristiche della rosetta sono le seguenti (capitolo 6.3):

- Misure e geometria della rosetta

  La rosetta ideale è circolare, con diametro di 800 μm;

- Tempo di completamento

  Tempo impiegato per il completamento della rosetta;

- Misura di penetrazione dello strumento

  Sotto la staffa ci sono le strutture dell'orecchio interno, importante parte per le funzioni dell'orecchio. Se lo strumento penetra troppo in profondità, rischia di danneggiare parti di tessuto; di conseguenza sarebbe ideale la minima profondità di penetrazione possibile. Il metodo usato per la misura della profondità di penetrazione è descritto nel capitolo 6.3.2;

- Caratteristiche del tremore

  Effetto del tremore sulla traiettoria dello strumento e precisione di manipolazione.

Risultati

Avendo documentato gli esperimenti con foto e video è stato possibile a posteriori l'analisi attraverso l'image processing delle rosette effettuate durante gli esperimenti. Differenti tecniche sono state utilizzate per il riconoscimento della forma della rosetta nelle prove con modello e con ossa da cadavere.

I parametri geometrici rilevati sono stati:

- Eccentricità (e) e rapporto d'aspetto
- Diametro equivalente
- Valore efficace del contorno ($RMS_{contour}$)

Inoltre anche altri parametri sono stati utili all'analisi:

- Percentuale di saturazione
- Valore efficace del tremore (RMS_{tremor})
- Massimo spostamento dovuto al tremore (Max_{tremor})
- Traiettoria della punta durante le bruciature laser

Le tecniche di image processing usate ed i parametri rilevati e calcolati sono descritti esaustivamente nel capitolo 6.3.1Mentre nelle sezioni del capitolo 7 i risultati sono presentati e brevemente commentati. Si riporta di seguito un breve riassunto:

- Dati geometrici

  Risultati opposti sono stati ottenuti dai due medici. Il chirurgo più esperto ha ottenuto risultati migliori senza l'aiuto di Micron (Micron off), mentre per il chirurgo più giovane è successo il contrario, avendo ottenuto rosette migliori nel caso Micron on. Il fatto di aver ottenuto risultati contrastanti può essere dovuto a molti fattori, che saranno discussi in seguito;

- Riduzione del tremore

  L'effetto della riduzione del tremore dato da Micron può essere osservato in Fig. 7.3. Micron aiuta a ridurre il tremore della punta per entrambi i chirurghi, sia nei test usando il modello che usando le ossa da cadavere;

- Effetti della cancellazione del tremore

  La parte volontaria è separata dal tremore attraverso un filtro: di conseguenza un ritardo è introdotto. Questo effetto si può vedere in Fig. 7.4 dove sono mostrati: il movimento della mano (impugnatura), posizione target (goal position) e la posizione attuale della punta. In Fig. 7.5 si vede invece l'effetto della cancellazione del tremore nella traiettoria della punta mente la rosetta viene effettuata: nel caso Micron on la traiettoria è molto più "pulita" ed efficace;

- Misura di penetrazione

  La profondità di penetrazione ottenuta nel caso Micron-on è risultata maggiore per entrambi i chirurgi contrariamente a quanto ci si aspettava. Da notare, tuttavia, l'elevato errore che affligge la misura. Questo è dovuto al metodo usato. Quindi non si possono trarre conclusioni riguardo la profondità, in quanto l'errore è troppo influente su tale misura;

- Tempo di completamento

  Il tempo di completamento nel caso Micron-on aumenta, anche se di poco. Ciò era atteso poiché per ottenere una cancellazione ottimale del tremore, l'utente deve manovrare lentamente lo strumento per permettere la cancellazione del tremore. Va anche tenuto in considerazione il range limitato di movimento dei motori che impedisce grandi e veloci movimenti.

Discussione

Nella discussione molti aspetti sarebbero da prendere in considerazione per spiegare la differenza che c'è stata tra i due chirurghi e perché non si è notata una grossa differenza tra i casi Micron on e off.

I principali punti di discussione e riflessione sono i seguenti:

- Esperienza del chirurgo e "allenamento" con Micron

  Sembra che Micron aiuti di più gli utenti con meno esperienza, che nel caso dei chirurghi significa i più giovani. Inoltre l'allenamento con Micron è fondamentale per capire come Micron risponde, imparare a muoversi lentamente e adattarsi al nuovo strumento. Il secondo chirurgo, più giovane e con più allenamento con Micron ha, infatti, ottenuto migliori risultati;

- Controllo del movimento e stanchezza

  Altra causa possibile della discordanza di risultati tra chirurghi potrebbe essere la stanchezza. Con il primo chirurgo, infatti, tutti gli esperimenti hanno avuto luogo la sera, a fine di giornata lavorativa. Questo significa stanchezza accumulata e minore concentrazione. Mentre con il chirurgo più giovane alcune prove sono state effettuate di prima mattina, quindi in condizioni ottimali. Come si può intuire la stanchezza è un fattore che influisce su tali prove essendo richiesta la massima precisione nei micro movimenti e la mano più stabile (senza tremore) possibile;

- Esperimenti con ossa da cadavere: incontrollate variabili introdotte

  Buona cosa durante gli esperimenti è avere il controllo su tutte le possibili variabili, e dunque possibili cause, durante lo

svolgimento. Alcune volte però ciò non è possibile. Questo è stato il caso negli esperimenti svolti con le ossa da cadavere: la staffa è un ossicino molto piccolo e quindi fragile. Durante la preparazione dell'osso, precedente gli esperimenti, il chirurgo ha dovuto rimuovere la parte superiore della staffa, lasciando in posizione solo la sua base. Durante quest'operazione la base della staffa può essere indebolita o fratturata, come poi è accaduto in alcune ossa usate. Il chirurgo quindi ha dovuto "operare" su una base fratturata e mobile (ossa senza otosclerosi), condizioni sfavorevoli per la buona riuscita dell'operazione. Tale fatto è dovuto anche alla limitata disponibilità di ossa da cadavere ed al loro costo;

- Uso dello speculum: vantaggi e svantaggi

  Lo speculum da un notevole vantaggio al chirurgo quando strumenti chirurgici tradizionali sono usati. I chirurgi, infatti, sono allenati a posare lo stelo dello strumento contro lo speculum che da supporto, permettendo di ridurre il tremore. Tale tecnica è però svantaggiosa quando Micron è usato: se la punta è posata contro lo speculum, i motori non riescono a muoversi liberamente e di conseguenza si saturano, producendo movimenti della punta innaturali e che possono rivelarsi dannosi.

  Per rimediare a ciò, come detto, si è sviluppata la protezione che permette al chirurgo di posare Micron allo speculum e contemporaneamente tenere la punta lontana dal suo bordo, permettendo ai motori una libera azione.

  Altro problema riscontrato è stato che così facendo, lo strumento è spostato più verso il centro dello speculum, ostruendo maggiormente il campo di veduta.

- Misura di profondità

  Come detto in precedenza la misura di profondità è affetta da un errore importante derivante dalla tecnica con il quale questa misura è stata rilevata. Di conseguenza non si possono trarre conclusioni se Micron aiuti o meno a ridurre la profondità raggiunta dallo strumento.

Tratte le conclusioni, è stata chiesta un'opinione anche ai chirurghi. Sono state evidenziate alcune problematiche da risolvere:

- Processo di calibrazione ogni qual volta lo strumento viene sostituito;
- Impedimento del movimento naturale in situazioni di saturazione e tocco dello speculum;
- Ostruzione del campo di veduta maggiore rispetto strumentazione convenzionale

Mentre punti di forza di Micron sono:

- Correzione del tremore che permette accuratezza di manipolazione e maggiore precisione se comparato con strumentazione convenzionale;
- Possibilità di usare Micron anche in altre operazioni chirurgiche all'orecchio o all'occhio, dove in molti casi si opera "a cielo aperto", quindi senza strumenti simili allo speculum che intralciano il movimento dei motori di Micron.

Tenendo conto di tutti questi fattori e delle limitazioni di Micron sono proposti alcuni sviluppi che in futuro potrebbero portare a un netto miglioramento dello strumento:

- Sviluppare un sistema di aggancio-sgancio rapido della strumentazione: in tale modo tutti gli strumenti che servono durante la chirurgia potranno essere usati e cambiati velocemente;
- Maggiore allenamento da parte degli utenti per capire esaustivamente il comportamento di Micron, anche in condizioni di saturazione;
- Sviluppare un sistema che permetta ai motori di continuare a operare indipendentemente se si verifica saturazione di uno di questi. Il movimento della punta dovrebbe essere comunque naturale e non pericoloso. Molto utile sarebbe anche un segnale sonoro per avvertire l'utente che sta saturando lo strumento;
- Rimpiazzare il sistema ASAP che richiede una chiara linea di visione tra i sensori PSD e le luci LED (avendo come conseguenza la limitata manovrabilità da parte dell'utente), con dei diversi sensori

per la posizione, che anche se meno precisi lasciano all'utente maggiore libertà di movimento.
- Modificare la protezione o gli strumenti per ridurre l'ostruzione del campo visivo;
- Ulteriore sperimentazione per avere una migliore valutazione del sistema.

Conclusione

Questo lavoro di tesi descrive il design, la prototipazione, il settaggio e l'adattamento di Micron, uno strumento attivo usato in otologia, in particolare per la chirurgia all'orecchio medio (stapedotomia).

Il primo passo è stato lo studio approfondito dell'operazione chirurgica stapedotomia. Dopodiché è stata sviluppata la strumentazione necessaria: un laser e uno strumento appuntito. Per prevenire il problema della saturazione e dare un punto d'appoggio all'utente, una protezione è stata sviluppata. Inoltre l'ergonomia è stata migliorata con una nuova impugnatura.

Dopo tali cambiamenti, la dinamica del sistema è cambiata, e quindi si sono dovuti settare i parametri di controllo. Per farlo l'identificazione del sistema dal punto di vista dinamico è stata fatta.

Una volta montata la nuova strumentazione e adattato i parametri di controllo si è passati alla sperimentazione per valutare le prestazioni del sistema. Esperimenti con il modello di orecchio e con ossa da cadavere sono sati svolti, con la partecipazione di due otorinolaringoiatri.

I dati e le immagini catturate durante gli esperimenti sono stati analizzati attraverso software di calcolo e image-processing.

Dai risultati di questo studio pilota riguardante l'uso di Micron nella stapedotomia si può dedurre che:

- Micron è stato maggiormente di aiuto per il chirurgo più giovane e quindi con meno esperienza;
- L'uso di Micron porta a movimenti più lenti, quindi il tempo di completamento delle fasi chirurgiche in cui Micron è usato aumenta, anche se di pochi secondi;

- La riduzione del tremore e una traiettoria più efficace della punta sono segno di un maggior controllo, con la minor possibilità di toccare tessuti delicati e quindi evitare complicazioni;
- L'allenamento con Micron è di fondamentale importanza: ciò aiuta a capire come si comporta Micron, per avere una manipolazione efficiente ed efficace;
- L'uso di Micron provoca un cambiamento nelle abitudini del chirurgo: non può, infatti, essere usato come uno strumento convenzionale.

Micron e la strumentazione sviluppata hanno ancora alcune problematiche da risolvere.

Tuttavia i risultati ottenuti sono promettenti e con sviluppi futuri sarà sicuramente possibile dimostrare i chiari vantaggi che questo strumento e questo approccio di cancellazione del tremore possono dare.

11 Bibliography

[1] S. Charles, D. Istrate, H. Das, T. Ohm, and C. Boswell, "Dexterity-enhanced Telerobotic Microsurgery," *Components*.

[2] C. J. Coulson and D. W. Proops, "ENT challenges at the small scale," no. April, pp. 91–96, 2007.

[3] C. J. Payne and G.-Z. Yang, "Hand-Held Medical Robots.," *Ann. Biomed. Eng.*, Jun. 2014.

[4] C. N. Riviere and N. V Thakor, "Modeling and Canceling Tremor in Human-Machine Interfaces," *IEEE Eng. Med. Biol.*, pp. 29–36, 1996.

[5] G. J. Tortora and B. Derrickson, *Principles of Anatomy and Physiology*, 12th editi. John Wiley & Sons, Inc., 2012.

[6] R. R. F. Ruby and R. H. Ballagh, "Reconstructive middle ear surgery." Canadina Family Physician, pp. 2689–2693, 1992.

[7] R. M. Farahani and M. Nooranipour, "Anatomy and anthropometry of human stapes.," *Am. J. Otolaryngol.*, vol. 29, no. 1, pp. 42–7, 2008.

[8] J. A. Shohet, "Otosclerosis," 15-Jul-2004. [Online]. Available: http://emedicine.medscape.com/article/859760-overview#showall.

[9] T. Kenny and J. Sambrook, "Otosclerosis," 15-Jul-. [Online]. Available: http://www.patient.co.uk/health/otosclerosis-leaflet.

[10] R. S. Haberman, *Middle Ear and Mastoid Surgery*. New York: Thieme, 2004.

[11] J. J. J. Shea, "Forty Years of Stapes Surgery," *Am. J. Otol.*, pp. 52–55, 1998.

[12] "Stapedotomy versus Stapedectomy." [Online]. Available: http://www.audiology.org/news/stapedotomy-versus-stapedectomy.

[13] M. Miroir, Y. Nguyen, J. Szewczyk, O. Sterkers, and A. Bozorg Grayeli, "Design, kinematic optimization, and evaluation of a teleoperated system for middle ear microsurgery.," *ScientificWorldJournal.*, vol. 2012, p. 907372, Jan. 2012.

[14] D. L. Rothbaum, J. Roy, D. Stoianovici, P. Berkelman, G. D. Hager, R. H. Taylor, L. L. Whitcomb, H. W. Francis, and J. K. Niparko, "Robot-assisted stapedotomy: micropick fenestration of the stapes footplate.," *Otolaryngol. Head. Neck Surg.*, vol. 127, no. 5, pp. 417–26, Nov. 2002.

[15] R. a Maclachlan, B. C. Becker, J. C. Tabarés, G. W. Podnar, L. a Lobes, and C. N. Riviere, "Micron: an Actively Stabilized Handheld Tool for Microsurgery.," *IEEE Trans. Robot.*, vol. 28, no. 1, pp. 195–212, Feb. 2012.

[16] B. R. C. B. Ecker, C. N. Riviere, and G. D. Stetten, "Vision-Based Control of a Handheld Micromanipulator for Robot-Assisted Retinal Surgery," Carnegie Mellon University, 2012.

[17] J. Binder and W. Kramer, "Robotically-assisted laparoscopic radical prostatectomy.," *BJU Int.*, vol. 87, no. 4, pp. 408–10, Mar. 2001.

[18] A. Parmar, D. G. Grant, and P. Loizou, "Robotic surgery in ear nose and throat.," *Eur. Arch. Otorhinolaryngol.*, vol. 267, no. 4, pp. 625–33, Apr. 2010.

[19] Y. Nguyen, M. Miroir, G. Kazmitcheff, E. Ferrary, O. Sterkers, and A. B. Grayeli, "From conception to application of a tele-operated assistance robot for middle ear surgery.," *Surg. Innov.*, vol. 19, no. 3, pp. 241–51, Sep. 2012.

[20] T. Maier, G. Strauss, M. Hofer, T. Kraus, A. Runge, R. Stenzel, T. Berger, A. Dietz, and T. C. Lueth, "A new Micromanipulator system for middle ear surgery," *IEEE Int. Conf. Robot. Autom.*, pp. 1568–1573, 2010.

[21] R. Taylor, P. Jensen, L. Whitcomb, A. Barnes, D. Stoianovici, Z. Wang, and L. Kavoussi, "A Steady-Hand Robotic System for Microsurgical Augmentation," vol. 18, no. 12, pp. 1201–1210, 1999.

[22] G. Stetten, B. Wu, R. Klatzky, J. Galeotti, M. Siegel, R. Lee, F. Mah, A. Eller, J. Schuman, and R. Hollis, "Hand-Held Force Magnifier for Surgical Instruments," pp. 90–100, 2011.

[23] D. Chang, G. M. Gu, and J. Kim, "Design of a Novel Tremor Suppression Device Using a Linear Delta Manipulator for Micromanipulation," pp. 413–418, 2013.

[24] S. Yang and C. N. Riviere, "Handheld Micromanipulator for Robot- Assisted Microsurgery," Carnegie Mellon University, 2014.

[25] W. T. Latt, C. Y. Shee, and W. T. Ang, "A Compact Hand-held Active Physiological Tremor Compensation Instrument," pp. 711–716, 2009.

[26] W. T. Latt, U.-X. Tan, C. Y. Shee, C. N. Riviere, and W. T. Ang, "Compact Sensing Design of a Handheld Active Tremor Compensation Instrument.," *IEEE Sens. J.*, vol. 9, no. 12, pp. 1864–1871, Dec. 2009.

[27] A. Saxena, S. Member, and R. V Patel, "An Active Handheld Device for Compensation of Physiological Tremor using an Ionic Polymer Metallic Composite Actuator *," pp. 4275–4280, 2013.

[28] C. Song, P. L. Gehlbach, and J. U. Kang, "Active tremor cancellation by a 'smart' handheld vitreoretinal microsurgical tool using swept source optical coherence tomography.," *Opt. Express*, vol. 20, no. 21, pp. 23414–21, Oct. 2012.

[29] F. Cepolina and R. Michelini, "Review of robotic fixtures for minimally invasive surgery," *Int. J. Med. Robot. Comput. Assist. Surg.*, vol. 01, no. 01, p. 43, 2004.

[30] R. J. Elble and W. C. Koller, "Tremor," *Johns Hopkins Univ. Press*, 1990.

[31] T. S. Wells, S. Yang, R. a Maclachlan, J. T. Handa, P. Gehlbach, and C. Riviere, "Comparison of Baseline Tremor Under Various Microsurgical Conditions.," *Conf. Proc. IEEE Int. Conf. Syst. Man. Cybern.*, pp. 1482–1487, Jan. 2013.

[32] R. a Maclachlan and C. N. Riviere, "High-Speed Microscale Optical Tracking Using Digital Frequency-Domain Multiplexing.," *IEEE Trans. Instrum. Meas.*, vol. 58, no. 6, pp. 1991–2001, Jun. 2009.

[33] G. Montes Grande, A. J. Knisely, B. C. Becker, S. Yang, B. E. Hirsch, and C. N. Riviere, "Handheld micromanipulator for robot-assisted stapes footplate surgery.," *Conf. Proc. IEEE Eng. Med. Biol. Soc.*, vol. 2012, no. c, pp. 1422–5, Jan. 2012.

[34] J.-P. Merlet, *Parallel Robots*, Second. Springer, 2006.

[35] B. Coleman and J. Babu, "One-Degree of Freedom Internal Model Control," in *Techniques of Model-based Control*, Prentice-Hall internationale series in the physical and chemical engineering sciences, pp. 39–64.

[36] MathWorks, “Color-Based Segmentation Using K-Means Clustering.” [Online]. Available: http://it.mathworks.com/help/images/examples/color-based-segmentation-using-k-means-clustering.html.

[37] S. Inc., “How to Analyze Data with Low Quality or Small Samples, Nonparametric Statistics.” [Online]. Available: http://www.statsoft.com/textbook/nonparametric-statistics. [Accessed: 20-Mar-2015].

March 2015

Tobia Vendrametto

tobia.vendrametto@gmail.com